UNIVERSIDADE DE SÃO PAULO

FACULDADE DE CIÊNCIAS FARMACÊUTICAS DE RIBEIRÃO PRETO

Structural studies on *Trypanosoma cruzi* nitroreductase enzyme: characterization of prodrug activation mechanism for benznidazole and nifurtimox

Estudos estruturais da enzima nitrorredutase de *Trypanosoma cruzi*: caracterização do mecanismo de ativação dos pró-fármacos benznidazol e nifurtimox

MARÍLIA DE LIMA CIRQUEIRA

Ribeirão Preto
2019

UNIVERSIDADE DE SÃO PAULO

FACULDADE DE CIÊNCIAS FARMACÊUTICAS DE RIBEIRÃO PRETO

MARÍLIA DE LIMA CIRQUEIRA

Structural studies on *Trypanosoma cruzi* nitroreductase enzyme: characterization of prodrug activation mechanism for benznidazole and nifurtimox

Estudos estruturais da enzima nitrorredutase de *Trypanosoma cruzi*: caracterização do mecanismo de ativação dos pró-fármacos benznidazol e nifurtimox

Master dissertation presented to the Graduate Program of School of Pharmaceutical Sciences of Ribeirão Preto/USP for the degree of Master in Sciences.

Concentration Area: Chemistry and Biological Physics

Supervisor: Prof. Dr. Maria Cristina Nonato

Co-Supervisor: Prof. Dr. Antônio José da Costa Filho

Corrected version of the Master's dissertation presented to the Graduate Program in Pharmaceutical Sciences on 02/08/2019. The original version is available at the School of Pharmaceutical Sciences of Ribeirão Preto.

Ribeirão Preto
2019

I AUTHORIZE THE REPRODUCTION AND TOTAL OR PARTIAL DISCLOSURE OF THIS WORK, BY ANY CONVENTIONAL OR ELECTRONIC MEANS

Cirqueira, Marília de Lima

Structural studies on *Trypanosoma cruzi* nitroreductase enzyme: Characterization of prodrug activation mechanism for benznidazole and nifurtimox. Ribeirão Preto, 2019.
75 p.; 30 cm.

Master dissertation presented to the Graduate Program of School of Pharmaceutical Sciences of Ribeirão Preto/USP for the degree of Master in Sciences. Concentration Area: Chemical and Biological Physics

Supervisor: Nonato, Maria Cristina

Co-supervisor: Costa Filho, Antônio José

1. Nitroreductase 2. Chagas disease 3. *Trypanosoma cruzi* 4. Membrane protein

APPROVAL PAGE

Marília de Lima Cirqueira

Structural studies on *Trypanosoma cruzi* nitroreductase enzyme: Characterization of prodrug activation mechanism for benznidazole and nifurtimox

Master dissertation presented to the Graduate Program of School of Pharmaceutical Sciences of Ribeirão Preto/USP for the degree of Master in Sciences.

Concentration Area: Chemistry and Biological Physics

Supervisor: Prof. Dr. Maria Cristina Nonato

Co-Supervisor: Prof. Dr. Antônio José da Costa Filho

Approved on:

Examiners

Prof. Dr. _____

Institution: _____ Signature:_____

Prof. Dr. _____

Institution: _____ Signature:_____

Prof. Dr. _____

Institution: _____ Signature:_____

Prof. Dr. _____

Institution: _____ Signature:_____

Agradecimentos

Gostaria de agradecer aos meus pais que me ensinaram que eu poderia fazer o que eu quisesse, mas que nada viria sem esforço. E além deles também aos meus irmãos, tios e tias, que cada um do seu jeito, me apoiaram e incentivaram nesse mestrado.

Ao meu namorado por me amparar nas inseguranças e sempre me incentivar.

À minha orientadora Cristina Nonato pela confiança em mim depositada, pelas correções que tanto me fizeram crescer e pelo apoio nas empreitadas.

Agradeço muito a todo time LCP-RP pelas discussões e teorias que me ajudaram na execução do meu projeto e companheirismo que tornou a caminhada mais agradável. Em especial a Iara e a Mariana pela amizade, paciência e pelas caronas.

Agradeço ao Professor Antônio José da Costa Filho pela disponibilização de equipamentos e materiais imprescindíveis para a conclusão deste trabalho e pelo auxílio na interpretação dos resultados.

Agradeço ao Professor Pietro Ciancaglini por disponibilizar o calorímetro de varredura diferencial e auxiliar nas interpretações dos resultados, juntamente com a Dra. Maytê Bolean.

Agradeço ao Professor Marcelo Dias Baruffi, pela disponibilização de equipamentos e materiais.

Gostaria de agradecer aos alunos do Laboratório de Biofísica Molecular, Laboratório de Nanobiotecnologia Aplicada: Sistemas Miméticos de Biomembranas e do Laboratório de Glicoimunologia que de uma forma ou de outra me ajudaram nas realizações dos experimentos e também pela companhia.

Agradeço à Professora Ana Paula Ramos por disponibilizar o tensiômetro OCA-20.

Agradeço à Professora Renata Viana Lopes por disponibilizar o equipamento Zetasizer.

Agradeço aos Professores João Santana e Ariel Silber pelo DNA genômico de *Trypanosoma cruzi* disponibilizado.

Agradeço ao Professor Shane Wilkinson por disponibilizar uma das construções gênicas utilizadas nesse trabalho.

O presente trabalho foi realizado com apoio da Coordenação de Aperfeiçoamento de Pessoal de Nível Superior – Brasil (CAPES) – Código de Financiamento 001.

“O correr da vida embrulha tudo, a vida é assim: esquenta e esfria, aperta e daí afrouxa, sossega e depois desinquieta. O que ela quer da gente é coragem.”

João Guimarães Rosa

Resumo

Cirqueira, M. L. **Estudos estruturais da enzima nitrorredutase de Trypanosoma cruzi: Caracterização do mecanismo de ativação dos pró-fármacos benznidazol e nifurtimox.** 2019. 75f. Dissertação (Mestrado). Faculdade de Ciências Farmacêuticas de Ribeirão Preto – Universidade de São Paulo, Ribeirão Preto, 2019.

A doença de Chagas é uma antropozoonose causada pelo parasita *Trypanosoma cruzi* e que afeta aproximadamente 5 milhões de pessoas somente na América Latina, causando, no mundo todo, cerca de 10 mil mortes por ano. A doença de Chagas crônica tem grande impacto social e econômico devido a morbidade relacionada a mesma. O benznidazol é atualmente o único medicamento disponível no Brasil para o tratamento da doença de Chagas. Usado há mais de 40 anos, é caracterizado por baixa efetividade na fase crônica da doença, alta toxicidade e casos de resistência já foram relatados. Estudos demonstraram que os compostos nitroaromáticos, como o benznidazol, são pró-fármacos ativados pela redução do grupo nitro, gerando metabólitos citotóxicos, uma reação que é catalisada pela enzima nitrorredutase do tipo I (TcNTR), ausente no hospedeiro humano. Apesar de inúmeros esforços da comunidade científica, a estrutura tridimensional da TcNTR, assim como as bases moleculares e químicas de ativação seletiva dos pró-fármacos são ainda desconhecidas. Nesse contexto, esse trabalho teve objetivo iniciar os estudos de caracterização da enzima TcNTR, através do uso de uma gama de técnicas biofísicas e bioquímicas. Duas diferentes construções, TcNTR72 e TcNTR78, foram expressas, purificadas e foram avaliadas com relação a estabilidade química e térmica por meio de técnicas de fluorimetria de varredura diferencial (DSF) explorando o grupo prostético endógeno mononucleotídeo de flavina (FMN) como a sonda fluorescente (ThermoFMN), e por espalhamento dinâmico de Luz (DLS). Nossos estudos mostraram que a construção TcNTR72 é mais estável e a presença do detergente triton X-100 é fundamental para a manutenção da integridade estrutural da proteína. Técnicas de calorimetria de varredura diferencial (DSC) e de tensiometria foram cruciais para demonstrar pela primeira vez a interação da TcNTR com membranas modelo que mimetizam a membrana interna mitocondrial. Estudos de modelagem molecular baseado em homologia e por métodos *ab initio* sugerem que a enzima TcNTR se enovela de forma similar às NTRs de bactéria. Domínios estruturais preditos como essenciais para a dimerização assim como o sítio do FMN localizado na interface dimérica foram identificados como conservados. A maior diferença entre a enzima TcNTR e as proteínas homólogas em bactérias aparece pela inserção de um fragmento de 23 resíduos na TcNTR, predito enovelar na forma de hélice-α. Com base em nossos resultados e nas diferenças em termos de localização celular e função entre as enzimas TcNTR e de bactéria, nossos estudos sugerem que a região pode ser importante para a interação da TcNTR com a membrana interna na mitocôndria do parasita. A alta identidade sequencial compartilhada entre as enzimas de tripanossomatídeos sugerem que nossos achados poderão ser extrapolados para o estudo das NTRs de outros parasitas como Leishmania *spp* e *Trypanossoma brucei*.

Palavras chave: Nitrorredutase, doença de Chagas, *Trypanosoma cruzi*, proteína de membrana.

Abstract

Cirqueira, M. L. **Structural studies on *Trypanosoma cruzi* nitroreductase enzyme: characterization of prodrug activation mechanism for benznidazole and nifurtimox.** 2019. 75f. Dissertation (Master). Faculdade de Ciências Farmacêuticas de Ribeirão Preto – Universidade de São Paulo, Ribeirão Preto, 2019.

Chagas disease is an anthropozoonosis caused by the parasite *Trypanosoma cruzi*, affecting approximately 5 million people in Latin America alone, and causing, worldwide, around 10 thousand deaths a year. Chronic Chagas disease have a major social and economic impact due to the disease causing disabilities. Benznidazole is currently the only drug available in Brazil for the treatment of Chagas disease. Used for more than 40 years, it is characterized by low effectiveness in the chronic phase, high toxicity and cases of resistance have been reported. Studies have shown that nitroaromatic compounds, such as benznidazole, are prodrugs activated by the reduction of the nitro group, generating cytotoxic metabolites, a reaction that is catalyzed by nitroreductase type I (TcNTR), absent in the human host. Despite several efforts by the scientific community, the three-dimensional structure of TcNTR, as well as the molecular and chemical bases of prodrugs selective activation are still unknown. In this context, this work aimed at initiating the characterization studies of the enzyme TcNTR, using a range of biophysical and biochemical techniques. Two different constructs, TcNTR72 and TcNTR78, were expressed, purified and evaluated for chemical and thermal stability by differential scanning fluorimetry (DSF), exploring the endogenous prosthetic group of flavin mononucleotide (FMN) as the fluorescent probe (ThermoFMN), and by dynamic light scattering (DLS). Our studies have shown that the TcNTR72 construct is more stable and the presence of the detergent Triton X-100 is critical for maintaining the structural integrity of the protein. Differential scanning calorimetry (DSC) and tensiometry techniques were crucial to demonstrate, for the first time, the interaction of TcNTR with model membranes that mimics the inner mitochondrial membrane. Homology and *ab initio* molecular modeling suggest that the folding of TcNTR is similar to bacterial NTRs. Structural domains predicted to be essential for dimerization as well as the site of FMN binding located at the dimeric interface were identified as conserved. The major difference between TcNTR enzyme and the homologous bacterial proteins appears to be the insertion of a 23 residues fragment in TcNTR, predicted to fold in the form of an α helix. Based on our results and the differences in cell localization and function between TcNTR and bacterial enzymes, our studies suggest that the region may be important for the interaction of TcNTR with the parasite inner mitochondrial membrane. The high sequence shared among trypanosomatid NTRs enzymes suggests that our findings can be extrapolated to the study of NTRs from other parasites such as *Leishmania* spp. and *Trypanosoma brucei*.

Key words: Nitroreductase, Chagas disease, *Trypanosoma cruzi*, membrane protein.

List of Figures

List of Tables

List of Abreviations

CL	Cardiolipin - 1,3-bis(sn-3'-phosphatidyl)-sn-glycerol
Cp	Calorific capacity
DLS	Dynamic light scattering
DPPC	1,2-dipalmitoyl-sn-glycero-3-phosphocholine
DPPE	1,2-Dimyristoyl-sn-glycero-3-phosphocholine
DSC	Differential scanning calorimetry
DSF	Differential scanning fluorimetry
DTT	Dithiothreitol
FMN	Flavin mononucleotide
IPTG	Isopropyl β-D-1-thiogalactopyranoside
kDa	KiloDalton
LB	Lysogeny brooth
NADH	Nicotinamide adenine dinucleotide
NTR	Nitroreductase
PDB	Protein Data Bank
PMSF	Phenylmethylsulfonyl fluoride
SUMO	Small Ubiquitin Modifier
Tb	*Trypanosoma brucei*
Tc	*Trypanosoma cruzi*
Tm	Melting temperature
ULP1	Ubiquitin like protease 1

Sumário

1. Introduction

1.1.Chagas Disease

Chagas disease or American trypanosomiasis is an antropozoonosis caused by the protozoan *Trypanosoma cruzi*, found naturally only in the American continent. Initially, it was believed that the *T. cruzi* clade evolved after the separation of South America and Africa. However, recent evidences indicate that *T. cruzi* evolved from a particular genotype found mostly in bats called TcBat and switched to terrestrial mammals through invertebrate vectors. *T. cruzi* has an extensive wild reservoir, especially mammals such as anteaters, armadillos, small primates and bats but there is no evidence of a negative impact in these natural hosts (GUHL; AUDERHEIDE; RAMÍREZ, 2014).

Chagas disease is pre-historical. Evidences suggests that human infections with *T. cruzi* occurred as soon as the South America was populated. The DNA of *T. cruzi* and classical signs of Chagas disease was found in a preserved mummy from 9000 years ago, where today is the south of Peru and the north of Chile. This finding generated the hypothesis that humans could have become hosts after the ingestion of the insect vector (triatomines) itself or the raw meat of infected animals. After the acquisition of sedentary habits and the domestication of animals, the triatomine vectors were attracted to live in the dwellings, made of mud and wood, initiating the domestic cycle of *T. cruzi* (ARAÚJO et al., 2009; STEVERDING, 2014).

Description of Chagas disease symptoms were found in records from travelers and physicians after the colonization of the American continent. However only in 1909 the Brazilian physician Carlos Chagas, in an expedition to the north of Minas Gerais state of Brazil, discovered the protozoan and named after his advisor, Oswaldo Cruz, as *Trypanosoma cruzi*. The flagellate was observed inside the hematophagous kissing bugs, abundant in that region, in the blood of domestic and wild animals, as well as, in infected patients with characteristic acute phase symptoms. Carlos Chagas described the transmission cycle, the vector, the etiological agent and the acute and chronic phase symptoms of the disease (COURA, 1997; KROPF, 2006; STEVERDING, 2014).

Chagas disease is endemic in Latin America where around 5 million people are infected, being a major public health problem (WHO, 2015). Only in Brazil, more than 1 thousand cases of acute Chagas disease were reported between 2012 and 2016. However, the real number can be substantially higher and underreported must be considered since the disease is not always identified in its acute phase (BRASIL, 2019).

Worldwide, around 10 thousand deaths a year is caused by Chagas disease (WHO, 2010). The economic burden is estimated in US$ 7.2 billion in health care costs and US$1.2 billion loss in productivity due to associated morbidity and mortality (LEE et al., 2013; STANAWAY; ROTH, 2015). The majority (90%) of the burden affects endemic countries and the major risk of infection is among underprivileged population with poor housing quality (LEE et al., 2013). The World Health Organization considers Chagas disease a neglected illness due to the lack of proportional investments to the the number of infected people, along with other parasitic diseases that affect mostly developing countries (WHO, 2010).

The life cycle of *Trypanosoma cruzi* involves distinct forms both in the insect vector and in the vertebrate host (Figure 1). The vectorial transmission occurs through cutaneous penetration of the metacyclic trypomastigote form, released in the feces of its vector, the triatomine insect, after its blood meal. Entering the bloodstream, the trypanosomatid is internalized by cells such as macrophages, muscle or nerve cells, developing intracellularly in their amastigote form and subsequently differentiating into trypomastigotes. These, after cell disruption, are released into the extracellular space, infecting new cells or infecting another triatomine during their blood meal (TEIXEIRA et al., 2012). During a process known as metacyclogenesis, bloodstream trypomastigotes differentiate into the replicative form named epimastigote in the host insect's stomach. After migrating to the insect's rectum, the epimastigotes differentiate into the non-replicative, infective metacyclic trypomastigote, completing the life cycle (GONÇALVES et al., 2018) (Figure 1).

After the discovery of the transmission cycle, several programs to control the disease insect vector were successfully implemented. Improvement of housing quality and application of insecticides led to the interruption of the transmission by the triatomine in most areas of Brazil (Figure 2). However, about 13% of Latin American population is still at risk of *T. cruzi* infection due to poor house conditions or active transmission (WHO, 2015).

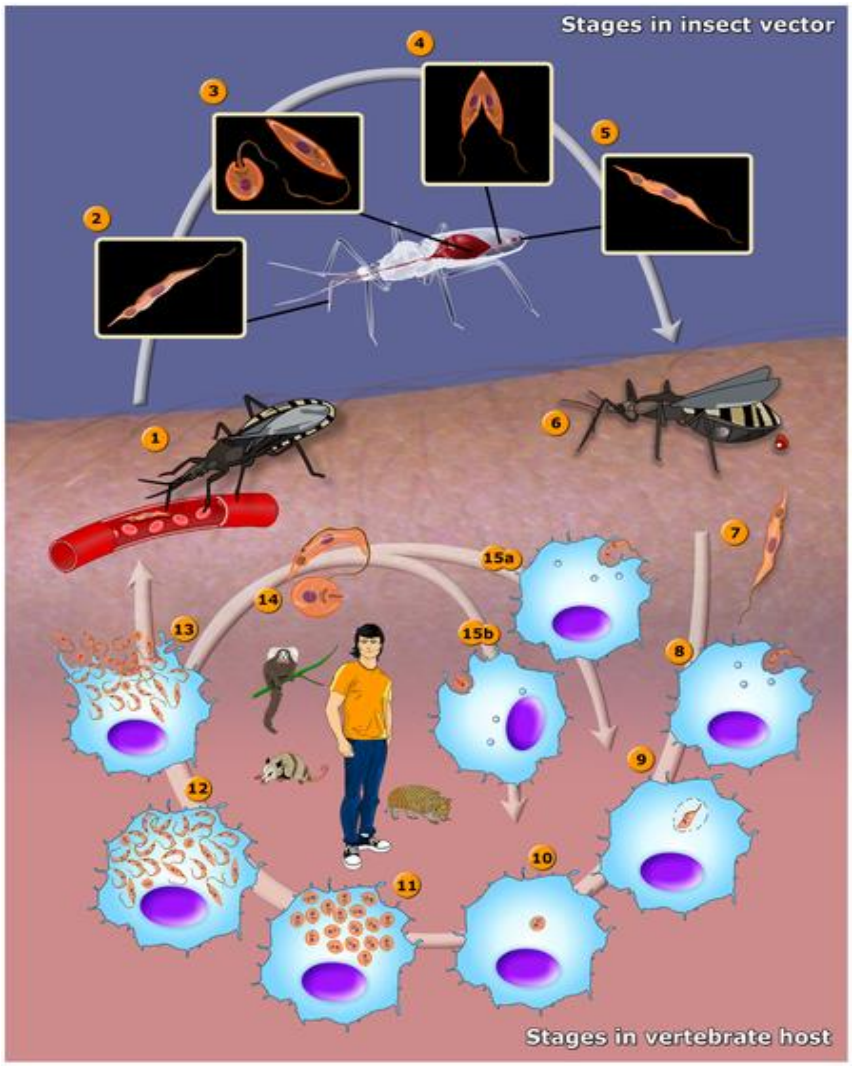

Figure 1: Schematic representation of the life cycle of *Trypanosoma cruzi*, etiologic agent of Chagas' disease: (1) infection of the triatomine by ingestion of trypomastigote forms; (2) metacyclic trypomastigote form; (3) differentiation in epimastigotes and spheromastigotes in the stomach; (4) binary division reproduction of the epimastigote forms in the intestine; (5) differentiation in metacyclic trypomastigotes in the rectum; (6) triatomine blood meal with elimination of the parasite by feces or urine; (7) metacyclic trypomastigotes enter the skin; (8) infection of macrophages with trypomastigotes; (9) lysosome containing the parasite; (10) differentiation into amastigotes; (11) multiplication of amastigotes in the cytoplasm; (12) differentiation into trypomastigotes; (13) rupture of the cell and release of trypomastigotes into the bloodstream; (14) amastigote and trypomastigote forms; (15) trypomastigotes (a) and amastigotes (b) infect new cells (Extracted from TEIXEIRA et al., 2012).

Nowadays, other forms of transmission, such as congenital, blood transfusion and organ transplantation, contributes to the spread of Chagas disease outside the endemic areas especially among migrant population (CONNERS et al., 2016; PÉREZ-MOLINA et al., 2015; ROBERTSON et al., 2016). This fact demanded the implementation of blood donor screening for *T. cruzi* DNA in the United States in 2007 (MARTIN et al., 2014).

Oral transmission, due to the ingestion of food contaminated with excrements or crushed parts of triatomines, has gained increased attention, and become a major issue in Brazil. It is found that 73% of Chagas disease acute cases reported between 2012 and 2016 were due to this type of transmission in Brazil (BRASIL, 2019).

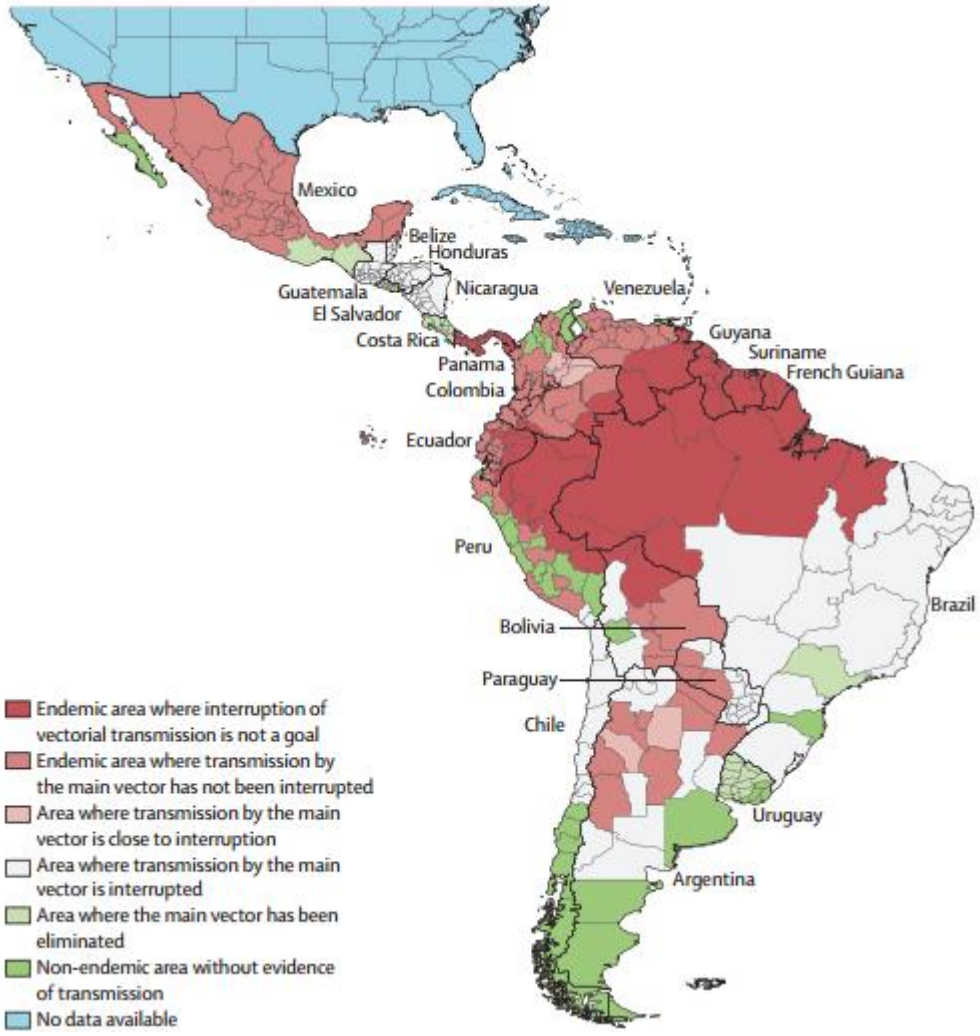

Figure 2: Current situation of Chagas disease in Latin America.(PÉREZ-MOLINA; MOLINA, 2017).

The clinical course of Chagas disease, composed by three phases, is highly related to genetic factors of the parasite and the host. The first phase, named acute, lasts around 2 to 4 weeks and presents unspecific symptoms, similar to those of other illnesses, such as fever and malaise. Despite being characterized by an abundant parasitemia that can be seen relatively easily by direct blood examination, the acute stage, in the majority of cases, is solved spontaneously, making its diagnosis very difficult. In only 2 to 3% of the cases, the acute phase can be life threatening due to acute myocarditis. The symptomatic acute phase is followed by an asymptomatic period of variable length that can last 10 years to life long and is characterized by non-detectable blood parasitemia. Reactivation of the acute phase can be observed due to

host compromised immune response related to other comorbities such as cancer and HIV infection (PEREZ; LYMBERY; THOMPSON, 2015). The last phase, named chronic, occurs in around 40% of infected people, characterized by cardiomyopathy and/or megagastrointestinal syndromes (PÉREZ-MOLINA; MOLINA, 2017).

A treatment for Chagas disease was made available only 50 years after the discovery of its causative agent. In 1966 benznidazole was released by Roche and later, in 1970, Bayer launched nifurtimox, which correspond to the only available drugs hitherto (Figure 3) (STEVERDING, 2014). Both compounds, however, cause harmful side effects ranging from cutaneous rash to blood marrow depletion. They have limited effectiveness in the chronic phase and resistant strains are reported. In Brazil only benznidazole is approved due to the higher toxicity displayed by nifurtimox (PÉREZ-MOLINA; MOLINA, 2017). Currently, an international multicentric trial called the BENEFIT project is evaluating the relevance of benznidazole treatment in late stage Chagas disease especially in patients with cardiovascular complications (MARIN-NETO et al., 2009). And nifurtimox, in combination with eflornithine is the recommended therapy for late stage African trypanosomiasis (HALL; BOT; WILKINSON, 2011a).

Benznidazole is a 2-nitroimidazole and nifurtimox a 5-nitrofuran. Thus, the chemotherapeutic potential of nitroheterociclics compounds, especially for trypanosomatid related diseases cannot be underestimated and should be exploited. These are considered prodrugs, being activated by the reduction of their nitro groups and formation of cytotoxic metabolites. This reaction occurs inside the parasites by an enzyme called nitroreductase (NTR) (WILKINSON et al., 2008).

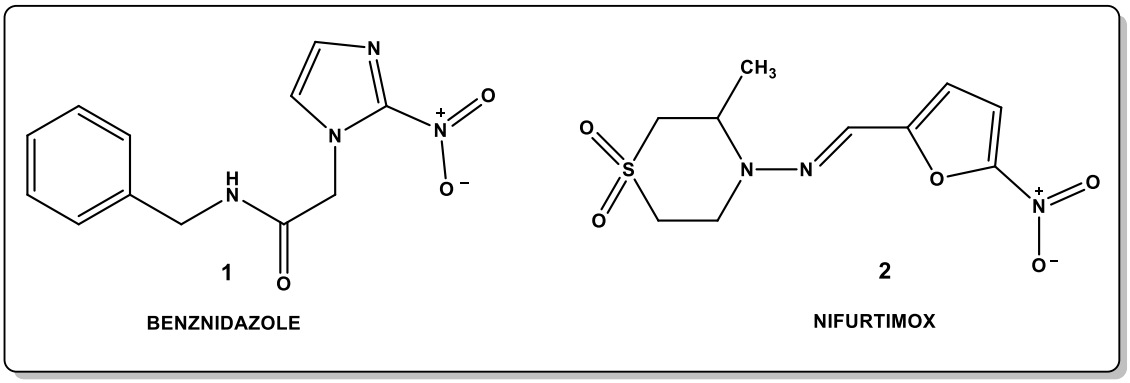

Figure 3: Chemical structure of the drugs benznidazole and nifurtimox.

1.2.Nitroreductases (NTRs)

NTRs are flavin dependent enzymes being classified into two categories, a type I, oxygen insensitive, promotes a sequential two-electron reduction in nitro groups to produce amine via hydroxylamine and nitroso derivatives, and type II, oxygen sensitive catalyze a one-eletron reduction into a nitro anion radical which can be reoxidized in the presence of oxygen to the nitro group, producing superoxide anions as a result of the futile cycle. Type I nitroreductases can be further divided into two groups, a group A nitroreductases are usually NADPH-dependent and share higher similarity with NfsA (oxygen-insensitive NADPH nitroreductase that reduces nitrofurazone) from *Escherichia coli*, and group B nitroreductases may use both NADH and NADPH as electron donors and are represented by *E. coli* NfsB (oxygen-insensitive NAD(P)H nitroreductase that reduces a variety of nitroaromatic compounds including nitrofurazone, quinones, nitroimidazoles, among others) (PATTERSON; WYLLIE, 2014; ROLDÁN et al., 2008).

Type I NTRs are mainly found in bacteria and some fungus species although protozoans such as *Trypanosoma* sp. and *Leishmania* sp. are exceptions believed to acquire this enzyme by lateral gene transfer (DE OLIVEIRA; HENRIQUES; BONATTO, 2007). The *T. cruzi* enzyme (TcNTR) is a type I nitroreductase that have a flavin mononucleotide (FMN) as prosthetic group, uses nicotinamide adenine dinucleotide (NADH) as a cofactor and is found in the large single mitochondrion of the parasite (WILKINSON et al., 2008a).

It has been observed that the induced loss of NTR genes in *T. cruzi* not only induced a higher resistance to benznidazole, nifurtimox and other nitro compounds but also decreased the growth rate of the parasites in its epimastigote form and prevented the differentiation into the infective form (metacyclic trypomastigotes), indicating an important metabolic role of TcNTR in the parasite. Also, the enzyme could not be deleted from blood stream forms of *Trypanosoma brucei* where the NTR could be essential for this stage form (WILKINSON et al., 2008a). The loss of NTR gene and its downregulation is also observed in *Trypanosoma cruzi* with induced resistance to benznidazole (MEJÍA-JARAMILLO et al., 2011). Nonsense and missense mutations have also been identified in drug-resistant parasites, although diverse mechanisms are involved in the resistance (CAMPOS et al., 2014; MEJIA et al., 2012).

A *T. cruzi* prostaglandin F2α synthase or old yellow enzyme (OYE) is a NAD(P)H flavin oxidoreductase that also mediates a type I reduction of nitrocompounds but only under anaerobic conditions *in vitro*. This enzyme has no homolog in *T. brucei* and is suggested that it participates in benznidazole activation along with TcNTR. TcOYE is overexpressed when

resistant parasites loses the NTR gene, and, under persistent drug exposure, the TcOYE gene is inactivated, being also involved in the mechanism of resistance (GARCÍA-HUERTAS et al., 2017; MURAKAMI et al., 2013). This way, NTR is believed to be the main activator of nitrocompounds used as prodrugs for Chagas disease.

For benznidazole, TcNTR and TbNTR promotes a serial 2 electron reduction in the drugs nitro group resulting in formation of nitrenium, dihydro-dihydroxy imidazole and glyoxal which reacts with thiols, proteins and nucleic acids causing cell damage (Figure 4). The redox reaction of the substrate follows a bi-bi ping pong mechanism of kinetics where initially the NADH is oxidized by the concomitant reduction of FMN. The nitrocompound is then reduced by $FMNH_2$, thereby regenerating oxidized flavin competent for further catalytic cycles (Figure 5) (HALL; WILKINSON, 2012; PATTERSON; WYLLIE, 2014).

In nifurtimox metabolism, unlike benznidazole, it is demonstrated the generation of superoxide anions. Until this moment, only NTR was confirmed to activate the drug but does not follow a classic ping pong kinetics, possibly due to more than one mechanism of activation. Nifurtimox also produces a hydroxylamine through a nitroso intermediate which can be further metabolized to a nitrenium ion or an open chain nitrile, which is highly toxic (even to mammalian cells) possibly due to non-specific reaction with a range of cellular molecules as it can function as a Michael acceptor (HALL; BOT; WILKINSON, 2011b).

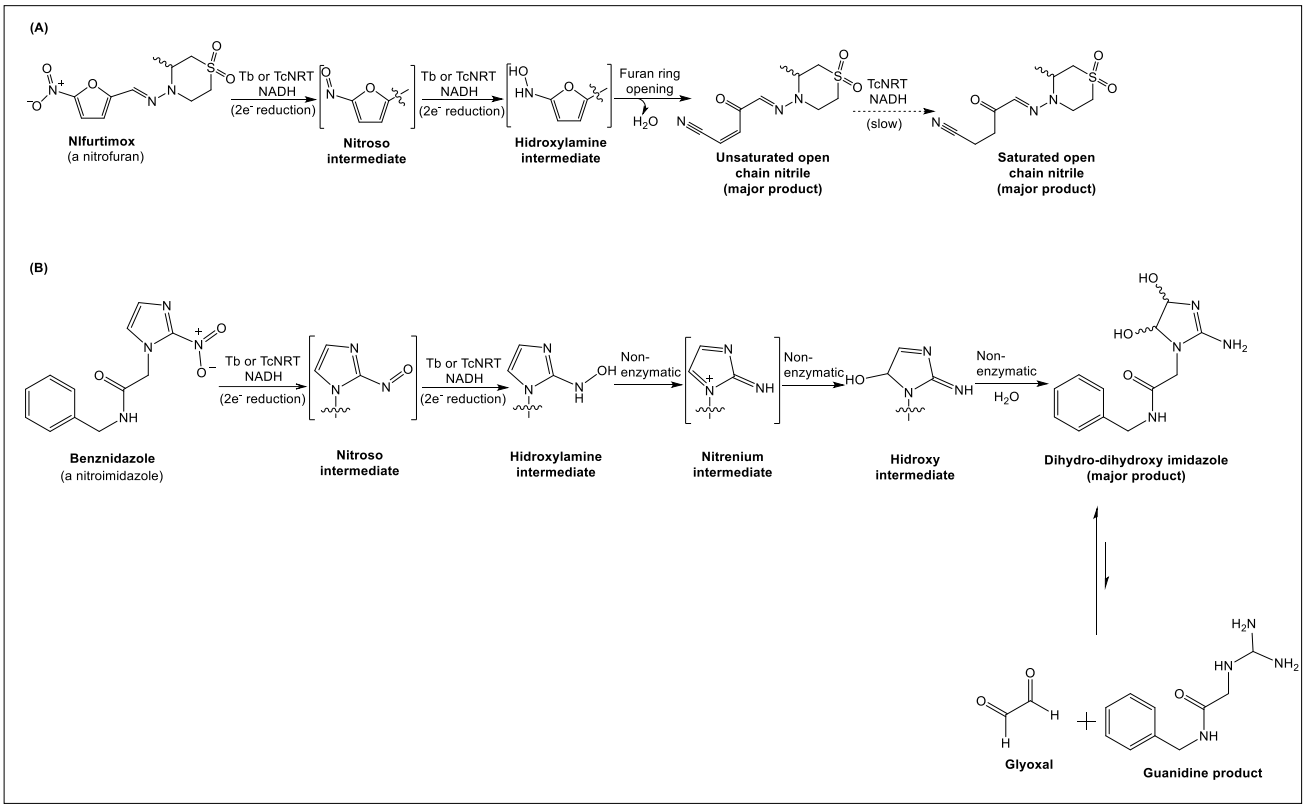

Figure 4: Schematic representation of the full reduction of the nitrocompounds benznidazole and nifurtimox by nitroreductases (Extracted from PATTERSON; WYLLIE, 2014).

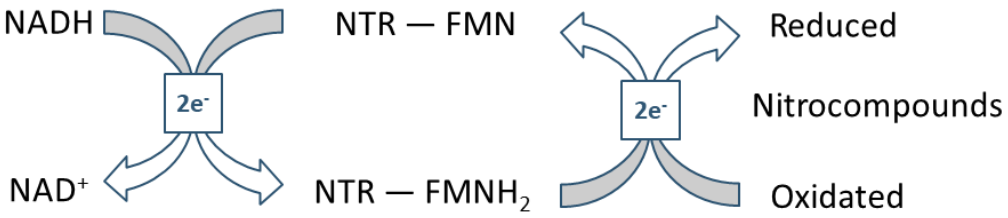

Figure 5: Representation of *T. cruzi* nitroreductase two substrate enzyme kinetics.

The exact physiological role of NTRs in bacteria or trypanossomatids is still unknown. In trypanosomes it is hypothesized that NTRs may function as ubiquinone reductases based on the mitochondrial location and preference for quinones. NTRs are also similar to FMN-dependent NADH dehydrogenases that reduces ubiquinone to ubiquinol using NADH as electron donor. This mechanism is essential in most organisms to maintain the NADH/NAD+ balance in mitochondrion and the redox balance in the cell. In trypanosomes, several NADH reductases are reported but mitochondrial energetics of these parasites is not fully discovered and considerably varies according to the parasite form (HALL; MEREDITH; WILKINSON, 2012; WILKINSON et al., 2008a).

Regarding its therapeutic role, nitroreductases are involved in the activation of metronidazole, a 5-nitroimidazole, in bacteria (NILLIUS; MÜLLER; MÜLLER, 2011; WANG et al., 2016). The enzyme is also related to metronidazole resistant strains of *Helicobacter pilory* (MARTÍNEZ-JÚLVEZ et al., 2012) and the protozoan *Giardia lamblia* (MÜLLER; HEMPHILL; MÜLLER, 2018). In addition, it is described the role of a type I nitroreductase in the inactivation of chloramphenicol conferring resistance of *Haemophilus influenza* (CROFTS et al., 2019). Nitroreductases are also studied as candidates for a directed enzyme prodrug therapy for cancer treatment (PROSSER et al., 2013).

They are often homodimers with subunits of 20 to 30 kDa, globular, with a conserved domain for FMN/FAD binding at the dimer interface using NAD(P)H as an electron donor. Nitroreductases possess a characteristic α+β-fold with a hydrophobic core of β-sheets surrounded by α-helices (Figure 6). The helix α6 is the responsible for the most of the dimer interactions along with the C-terminal portion that protrudes around the opposing monomer. The region comprising the α4 and 5 is flexible, important to accommodate the different substrates described. The low identity between NTRs of trypanosomatids and bacteria can also explain the selectivity to different nitrocompounds (ROLDÁN et al., 2008).

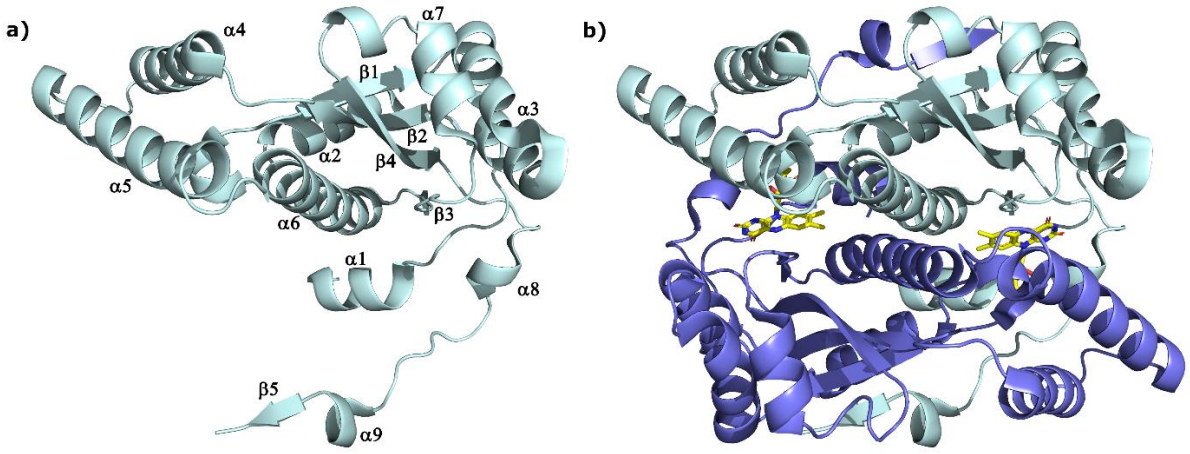

Figure 6: Cartoon representation of *E. coli* nitroreductase (PDB code: 1DS7) monomer (a) and dimer (b).

A type I NTR is absent in the human host which makes it an interesting target for new trypanocidal drugs. The side effects observed for the available drugs are a result of non-specific reduction by human enzymes (such as alcohol dehydrogenase 2 and P450 oxidoreductase) and metabolization by the intestinal microbial communities, which is determinant for toxic metabolism of pollutant chemicals (HUNTER et al., 2015; PATTERSON; WYLLIE, 2014; ROLDÁN et al., 2008; ZHOU et al., 2012).

Considering the high number of infected people, the toxicity and lack of efficacy of available drugs, other therapeutic options must be searched. One possible strategy is to identify and characterize potential macromolecular targets for the development of new therapies. This work focuses on the characterization of TcNTR. The results of our studies will not only contribute to map the mechanism of activation of the available pro-drugs but also contribute to understand the role of NTR in *Trypanosoma cruzi*. Hence, a better evaluation of NTR structure is fundamental to the development more specific and effective drugs.

2. Objectives

This project aims at obtaining recombinant *Trypanosoma cruzi* nitroreductase enzyme in the soluble form, functionally active, stable and with good yield, and at characterizing it by combining biochemical and biophysical approaches. In order to achieve this goal, the following steps must be accomplished:

- Standardize the heterologous expression of two different constructs in *E. coli* and purify two enzyme fragments: TcNTR78 (78-312) and TcNTR72 (72-312) in a soluble and active form;
- Characterize the biophysical properties of TcNTR78 (78-312) and TcNTR72 (72-312) fragments, using differential scanning fluorimetry (DSF), dynamic light scattering (DLS) and differential scanning calorimetry (DSC);
- Perform structural studies by exploiting single crystal X-ray diffraction and molecular modeling techniques.

3. Materials and methods

3.1. Cloning

The construct named hereafter TcNTR78 was generously donated by Professor Shane Wilkinson from the Queen Mary University (London – England). It comprises residues from 78 to 314 (Figure 7) inserted into a pTrcHis-C vector (Invitrogen). In this construct, TcNTR is expressed as a polyhistidine-tagged fusion protein that facilitates protein purification by making use of affinity chromatography.

The construct TcNTR72 was cloned in our laboratory by the PhD student Mariana Araújo Ajalla Aleixo. The genomic DNA from *Trypanosoma cruzi* Y epimastigotes (kindly

donated by Professor João Santana and Ariel Mariano Silber) was used as a template for fragment amplification. The primers forward and reverse were designed with BamHI and XhoI restriction sites, respectively, both underlined: *gac gac gga tcc TCA TCA TCA TCA TTG CCG* and *gac gac ctc gag TCA AAA CTT TCC CCA CC*. The TcNTR72 was inserted into a pET28a-SUMO vector (Novagen) for expression. In this construct, TcNTR72 is expressed as a N-terminal fusion-tag enzyme, containing a small ubiquitin-like modifier protein (SUMO, 12 kDa) and a histidine tag. The SUMO tag is believed to enhance protein stability and can be removed by cleavage by ubiquitin like specific protease 1 (ULP1), leading to an untagged protein (MARBLESTONE, 2006).

3.2. Expression

Expression of TcNTR gene fragments were initially performed by testing different *E. coli* strains: BL21 (DE3), Rosetta ™ (DE3) and Codon plus and different isopropyl β-D-1-thiogalactopyranoside (IPTG) concentrations (from 100 to 500 μM). Protein expression was analyzed by 14% SDS-PAGE.

Competent strains were transformed by heat shock. Then 300 ng of the plasmid containing the target protein were added into 50 μl of the suspension of competent cells and gently homogenized. The mixture was incubated on ice for 30 minutes, followed by a 2 minute heat shock at 42 ºC and 5 minutes on ice. 250 μl of Luria Bertani liquid culture medium (LB) was added to the suspension and the mixture was incubated at 37°C under shaking at 180 rpm for 1 hour. After this time, 80 μl of the cell suspension were seeded in a Petri dish with solid LB medium, previously treated with the appropriate antibiotics for each construct (34 μg/mL of chloramphenicol and 100 μg/mL of ampicillin for TcNTR78; 30 μg/mL of kanamycin and 34 μg/mL chloramphenicol for TcNTR72). The plate was incubated in a bacteriological oven at 37 °C for 16 hours.

When using IPTG to induce protein expression, the pre-inoculum was cultured with enriched LB medium with sodium chloride (85 mM) and magnesium sulfate (16.61 mM) with the adequate antibiotics (34 μg/mL chloramphenicol and 30 μg/mL of kanamycin). It was let grow at 37 °C, for 16 hours under constant stirring at 180 rpm. The culture was diluted 1:50 in the enriched media containing the appropriate antibiotics and incubated at 37 °C with stirring at 180 rpm for 2 hours. The suspension then was let cool to 17°C and until the optical density reached between 0.7 and 0.8 u.a. at 600 nm when 300 μM of IPTG was added. The culture

remained at 17 °C under constant stirring (180 rpm) for 20 hours. Cells were collected by centrifugation at 8,000 x*g* at 4 °C and stored at -20 °C.

Protein production by auto-induction followed a protocol described by Studier (2005). Competent strains of *E. coli* Rosetta were transformed with the plasmid as described before. The growth medium for high density cultures, ZYM-5052, contained 1% of tryptone, 0.5% of yeast extract, 25 mM of Na_2HPO_4, 25 mM of KH_2PO_4, 50 mM of NH_4Cl, 5 mM of $NaSO_4$, 2 mM of $MgSO_4$, 0.5% (v/v) of glycerol, 0.05% (v/v) of dextrose and 0.2% (v/v) of α-lactose. The pre-inoculum prepared with LB media and antibiotics was diluted in a 1:1000 rate into 50 mL of ZYM-5052 containing 34 μg/mL chloramphenicol and 100 μg/mL of kanamycin (the increased concentration of the later antibiotic is due to resistance caused by the high phosphate concentration in the medium) in a 1 L Erlenmeyer. The cultures were kept at 37 or 20ºC under stirring at 200 rpm until saturation. After optimization of the expression protocol, protein expression was standardize to be performed at 20ºC for 48 hours in a 2 L vessel, which was used for 300 mL of cell culture.

3.3. Purification

Cells were resuspended in the lysis buffer with added protease inhibitor phenylmethysulfonyl fluoride (PMSF) (50 mM Tris, pH 8.5, initially 500 mM NaCl, 1 mM DTT, 1 mM PMSF and 1% Triton). Alternatively it was also added 10% glycerol. The suspension was sonicated at 10 W in 15 cycles of 30 seconds pulses and intervals of 30 seconds in ice. After centrifugation at 16,000 x*g* for 30 min at 4 ºC, the supernatant was separated and applied into a Poly-Prep® column packed with 2 mL of Ni-NTA resin (Quiagen) pre-equilibrated with binding buffer (50 mM Tris, pH 8.5, initially 500 mM NaCl, 0.5 mM DTT, 0.1% Triton). For removal of contaminants, the column was washed with binding buffer in presence of an increasing gradient of imidazole (0 and 50 mM imidazole).

Purified TcNTR78 protein was then eluted in presence of 500 mM imidazole. Samples were combined, dialyzed and concentrated in a 10 kDa cutoff Amicon Ultra Spin column.

Pure TcNTR72 was eluted in presence of 250 mM imidazol and submitted to dialysis for imidazole removal prior to cleavage of tag SUMO protein using 50 U of the ULP-1 enzyme for 4 hours. Both polyhistidine-tagged SUMO protein and ULP-1 were separated from the pure untagged TcNTR72 by reapplying the digested mixture into the Ni-NTA affinity column. Purity was confirmed by polyacrylamide gel electrophoresis (14%).

3.4. Determination of protein extinction coefficient based on prosthetic group FMN.

Protein concentration was determined based on the molar extinction coefficient from the prosthetic group FMN in a U2900 spectrophotometer (Hitachi – Tokyo, Japan). Initially, 600 µL of pure protein samples were scanned within the visible region of the spectrum and the maximum absorbance found in 461 nm recorded ($Abs_{max.enz.}$). The scanned samples were then heated to 80 °C for 15 min followed by centrifugation at 16,000 xg for 10 min. The yellow supernatant containing free FMN was separated from the insoluble fraction, scanned, and the maximum absorbance at 446 nm recorded. The enzyme extinction coefficient was determined considering equimolar concentrations of free and enzyme-bound FMN (Equation 1). The FMN extinction coefficient of ε_{FMN}= 12,200 mol^{-1} L cm^{-1} was used as reference (CHAPMAN; REID, 1999).

$$\varepsilon_{ENZ} = \frac{Abs_{max.enz.} x\ \varepsilon_{FMN}}{Abs_{446FMN}} \qquad \text{(Equation 1)}$$

3.5. Activity test

Both constructs had their activity tested by measuring the oxidation of NADH by decreasing the absorbance at 340 nm. The reaction mixture contained 50 mM of Tris pH 7.5, 75 µM of NADH and 50 µM of benznidazole, which were incubated at room temperature for 5 minutes. The oxidation reaction started with the addition of 20 µg/mL of TcNTR.

3.6. Evaluation of protein thermal stability

Thermal stability was evaluated by using differential scanning on the fluorescence of the NTR prosthetic group FMN also called ThermoFMN (PÁDUA et al., 2014). It was developed by our research group as an adaptation of the technique developed by Pantoliano and coworkers (2001), in which the fluorescence observed comes from a probe added to the solution.

In this assay, the temperature is raised from 25 ºC to 95 ºC in a rate of 1 ºC/minute. The gradual increase in temperature will force the unfolding of the protein, exposing its prosthetic group and generating a fast increase in the florescence, resulting in a sigmoidal curve. The

midpoint temperature is called melting temperature (Tm), the transition temperature between the folded and unfolded states and is calculated using a Boltzmann sigmoid equation.

$$I = \left(A + \frac{(B-A)}{1+ e^{(Tm-T)/C}}\right) \quad \text{(Equation 2)}$$

Different buffers, salt concentrations and additives can increase or decrease protein organization and consequently its stability. This affects the Tm causing a shift (ΔTm), positive or negative. The unfolding of the protein is a cooperative process, thus, ideally, the thermal denaturation should be fast and a high slope of the fluorescence curve observed (BOIVIN; KOZAK; MEIJERS, 2013; ERICSSON et al., 2006; SANTOS et al., 2012).

The assays were performed in a real time PCR - Mx3005P (Agilent Technologies – Santa Clara, CA – USA) coupled with a FAM SYBR GREEN filter, adequate to monitor the fluoresce of FMN (excitation at 492 nm and emission at 516 nm {PÁDUA et al., 2014}). Solubility and Stability Screen 1 and 2 and Detergent Screen from Hampton Research (Aliso Viejo, CA – USA) was also used to evaluate the influence of different pHs, buffers, salt and additives in the Tm. Typical assay volumes were 20 µL containing 2 µL of protein sample in a concentration of approximately 1 mg/mL.

3.7. Evaluation of protein solution dispersity

DLS is a technique used for estimating the dispersity of a sample in solution and the hydrodynamic radii of its different components. This technique operates on the principle that particles move randomly in gas or liquid i.e. undergo Brownian motion. The movement (diffusion) of these particles is described by the Stokes-Einstein equation (equation 3)

$$D = k_B T/6\pi nR \quad \text{(Equation 3)}$$

where the diffusion (D) is equal to the product of Boltzman's constant (k_B) divided by the hydrodynamic radius of the particle (R) of the particle and the shear viscosity of the solvent (n). Larger particles have a slower velocity and will have smaller coefficients of diffusion than larger particles (KASZUBA et al., 2008).

During DLS experiments, a laser is shined through the sample and the molecules in free movement scatter radiation in all directions, which interferes constructively and destructively. During the experiment, the scattered light is monitored and the hydrodynamic radio is determined, derived from the diffusion coefficient of the protein molecules.

The technique is non-destructive and uses a small volume of sample that does not necessitate any modification (HAWE et al., 2011). In our experiments we utilized a Zetasizer Nano ZS (Malvern Instruments) using the quartz cuvette ZEN 2112 (Hellma®). 50 μL of protein sample in a concentration ranging from 0.6 to 1.2 mg/mL is equilibrated for 60 s at 16 ºC, exposed to the laser beam for 10 s and the scattered light was monitored at 90º. The numberof runs for each measure was optimized by the Zetasizer Software. The model of analysis wasprovided by the software being specific for proteins, which uses a standard regularized non-negative least squares analysis. The profile shown was built as an average of 3 measures.

3.8. Evaluation of salt concentration on protein stability

In order to determine the influence of salt concentration on protein stability, the construct TcNTR72 was initially used. Purified protein was initially dialyzed against 50 mM Tris pH 8.5, 0.5 mM DTT, 0.1% Triton, and 100 mM NaCl. The sample was separated in small aliquots, with increasing salt concentration (100, 200, 300, 500 mM), and analyzed by DSF and DLS. For DSF 2 μL of the samples (0.7 mg/mL) were diluted to 20 μL of water and the fluorescence monitored from 25 to 95 ºC in a rate of 1 ºC/minute. For DLS, 50 μL of protein solution at a concentration of 0.7 mg/mL were measured at 16 ºC with the number of 10 s runs optimized by the Zetasizer Software.

3.9. Evaluation of Triton X-100 on protein stability

In order to evaluate the influence of the detergent Triton X-100 on protein stability, a complete purification protocol of TcNTR72 construct was conducted in absence of this additive. All the other components and the purification protocol were kept unchanged. Protein was analyzed by DLS, at 16 ºC with the number of 10 s runs optimized by the Zetasizer Software.

3.10. Crystallization experiments

X ray crystallography is a tool that provides atomic level information on protein structures, which have been fundamental for understanding diverse biological processes (BERGER et al., 1996; GARCIA-GUERRERO et al., 2018; MCCUSKER et al., 2012). The disadvantage of the technique is the requirement of protein solutions highly concentrated and stable.

Crystallization experiments were carried out with the construct TcNTR72 due to its higher stability and lower dispersity. Prior to crystallization experiments, the purified protein was submitted to a size exclusion chromatography using a Superdex 200 10/300 column (GE Healthcare – Hungary) pre-equilibrated with 50 mM of Tris pH 8.5, 300 mM NaCl, 0.1% Triton X-100. The fractions from the homogeneous peak were pooled, concentrated and incubated for 1 hour in presence of different detergents and additives.

Table 1: Protein solution conditions tested for crystallization in sparse matrix commercial kits and optimization attempts.

	Conditions tested	
Protein	**Detergent**	**Additive**
Tag free protein (5 and 10 mg/ml)	N,N-dimethyldodecylamine N-oxide – DDAO (10 mM)	Free FMN (1mM) + benznidazole (1mM)/ NADH (1mM)
Tag free protein (5 and 10 mg/ml)	N,N-dimethyldodecylamine N-oxide – DDAO (10 mM)	Benznidazole/NADH (1mM)
Protein with sumo tag (5 mg/ml)	N,N-dimethyldodecylamine N-oxide – DDAO (10 mM)	Benznidazole/NADH (1mM)
Tag free protein (5 mg/ml)	n-octil-β-D-glucosamide - OG (10 mM)	Benznidazole/NADH (1mM)
Tag free protein (5 mg/ml)	1-palmitoyl-2-hydroxy-sn-glycero-3-phosphocholine – 16:0 LysoPC	Benznidazole/NADH (1mM)
Tag and detergent free (5 mg/ml)	-	Benznidazole/NADH (1mM)
Tag free protein (5 and 10 mg/ml)	1-palmitoyl-2-hydroxy-sn-glycero-3-phosphocholine – 16:0 LysoPC	None.

Initial crystallization conditions were screened by the sparse matrix method (Jancarik & Kin, 1991) using the commercially available screening kits: Crystal Screen, Index, PegRx, PegIon from Hamptom Research (USA), Pi minimal and JBScreen Membrane from Jena

Bioscience (Germany). The method used was the sitting-drop vapor diffusion technique using a 96-well plates (*SWISSCI MRC 2 Well*, *Jena Bioscience*, Germany) and a drop settler for protein crystallization NT8 (Formulatrix – Bedford, USA). Equal volumes (100 nL) of protein and reservoir solution were mixed, equilibrated against 100 μL of reservoir solution and kept at 293 or 277 K. Additional efforts were made in order to optimize the crystal quality by screening various crystallization variables (pH, precipitant concentration, temperature and additives).

3.11. Protein-membrane interaction

Interaction between TcNTR with membranes were evaluated by differential scanning calorimetry (DSC), pendant drop tensiometry and fluorescence spectroscopy.

3.11.1. Differential Scanning Calorimetry

Differential scanning calorimetry (DSC) is an analysis that measures the changing in physical properties of a variety of materials by the temperature range at a constant pressure. As the temperature increases, thermally induced processes in the sample results in heat absorbance or release, which generates a difference in temperature relative to a reference. In order to minimize the temperature difference between the cells, a compensating power is applied to the sample. The data is normalized based on the sample concentration, cell volume, and scan rate, in order to calculate the excess heat capacity of the sample, Cp (kcal/K.mol), as function of temperature (ºC) (the heat input required to raise the temperature by one degree) (DEMETZOS, 2008; DUROWOJU et al., 2017; JOHNSON, 2013; SPINK, 2008).

Liposomes are spherical lipid bilayers often used as models to mimic cellular membrane. With the addition of thermal energy, the alkyl chains from the phospholipids transit from a *trans* conformation, called gel phase (L_{β}), to a *gauche*, disordered conformation, the liquid-crystalline phase (L_{α}), affecting the van der Waals interactions between the phospholipids hydrocarbon chains (Figure 7). When used in DSC, information on the thermotropic behavior of the lipid system in diverse environments, such as different lipid compositions, pHs, ionic strength and presence of ligands, is acquired. The temperature, enthalpy, and entropy of the phase lipid transition may be affected by differences in lipid-lipid interactions and due to protein-lipid interaction. This way, DSC is an appropriate tool for

analyzing the influences of a membrane protein in a lipid system (DEMETZOS, 2008; DRAZENOVIC et al., 2015; SPINK, 2008).

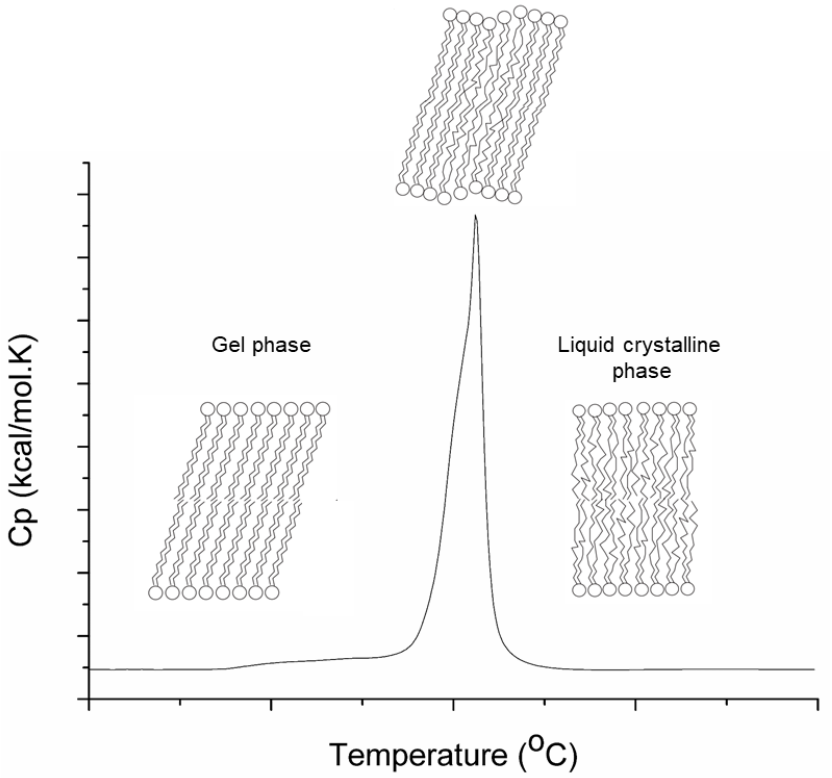

Figure 7: Scheme presenting a typical thermogram of a lipid phase transition and the effect of temperature in the acyl chains (Adapted from DEMETZOS, 2008).

The lipid 1,2-dipalmitoyl-sn-glycero-3-phosphocholine (DPPC, 16:0 PC, Sigma), were used as preliminary models for our studies. The lipid was solubilized with chloroform and the dry lipid film were formed after evaporation under a stream of nitrogen and in a vaccum chamber overnight. The film was ressuspended in 50 mM Tris pH 8.5, 300 mM of NaCl to a final concentration of 4 mM and incubated at 55 ^{o}C for 1 hour, above the critical phase transition temperature of the lipid, and vortexed for each 10 minutes. The formed multillamelar vesicles were extruded using a 100 nm polycarbonate filter in an Avanti Mini-Extruder (Avanti Polar Lipids - USA). The physical status of the liposomes and the interference of the protein were checked by measuring the size distribution using DLS (N5 Submicron Particle Size Analyzer – Beckman Counter – Pasadena, EUA). The DSC analysis was performed in a calorimeter N-DSC II at Professor Pietro Ciancaglini lab (Calorimetry Science Corporation – Lindon, USA).

DPPC was the lipid of choice for studies using different protein:lipid ratios (1:90000, 1:45000 in molar) and incubation time (1, 2, 5 and 12 hours). The detergent was removed using the Calbiosorb resin to minimize the possible interference of its presence.

To remove excess detergent, 1mL of Triton X-100-solubilized protein (approximately 1% of detergent) was added to 500 mg of Calbiosorb resin and the suspension was mixed gentle for 5 minutes at 4 °C and the process is repeated. The supernatant is the source of detergent-free solubilized protein. The TcNTR72 protein concentration was quantified using the Hartree method (HARTREE, 1972).

In order to mimics the inner mitochondrial membrane, combinations of the lipids DPPC, DPPE (1,2-dipalmitoyl-sn-glycero-3-phosphoethanolamine, 16:0 PE, Avanti Polar Lipids) and cardiolipin (CL, 1,3-bis(sn-3'-phosphatidyl)-sn-glycerol, Sigma) were used with the molar proportion of 1:168 of protein:lipid. The combination DPPC:DPPE:CL in the molar ratio of 2:1:1 were already reported as a suitable model (CHENIOUR et al., 2017).

Thermograms (calorific capacity versus temperature) of purified TcNTR72 protein were also made in the presence and absence of the detergent Triton X-100 in the concentrations of 0.25, 0.5 and 0.95 mg/mL.

3.11.2. Pendant drop tensiometry

The pendant drop tensiometry measures the interfacial tension of a drop suspended from a needle, being a simple and versatile method. It is based in the axisymmetric drop shape analysis (ADSA) in which the shape of the pendant drop is related to is interfacial tension using the Young–Laplace equation (BERRY et al., 2015; SAAD; POLICOVA; NEUMANN, 2011). The technique has many applications and among them is the possibility to access the capacity of a protein to penetrate the lipid film where a monolayer serves as a membrane model and is formed in the air-water interface (Figure 8). The insertion of the protein into the membrane results in an increase of the surface pressure, which is the difference between the surface tension of pure water and surface tension after the phospholipids and protein addition. (ANDRADE et al., 2016; WEINBERG et al., 2002).

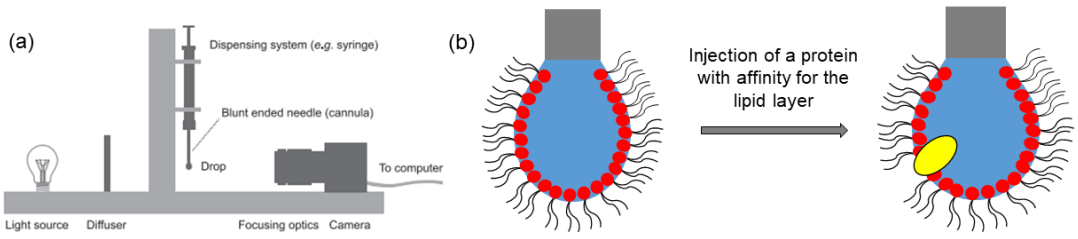

Figure 8: Schematic representation of (a) basic pendand drop tensiometry experimental setup (BERRY et al., 2015) and (b) the basis of ADSA.

For measuring the surface tension an automatic tensiometer OCA-20 (Dataphysics) was used with drop volumes varying between 10 and 13 μL. The reference used was the buffer composed of 50 mM Tris pH 8.5 and 300 mM of NaCl. The lipid monolayer was formed by injection of a few microliters of a chloroformic solution of the chosen lipids inside the drop until achieved an initial interfacial pressure of 5, 10, 15 and 20 mN/m. After the stabilization of the drop, 0.5μL of TcNTR72 (detergent-free solubilized protein) at a concentration of 0.8 mg/mL was injected inside the drop and the increase in the surface pressure monitored until reaching a stable plateau ($\Delta\pi$). The exclusion pressure of the construct TcNTR72 was determined by extrapolation of the maximum surface pressure increase *versus* the initial pressure of the lipid monolayer.

3.11.3 Fluorescence spectroscopy

The fluorescence of the prosthetic group FMN was recorded in a Hitachi F-7000 fluorescence spectrophotometer at room temperature. The excitation wavelength was 450 nm and the emission recorded between 480 and 600 nm with emission and excitation slits of 5 nm. Unillamelar liposomes of DPPC were made as previously described at final concentrations of 1, 0.5 and 0.25 mM. The TcNTR72 solution (2 mg/mL) had the detergent withdrawn and was incubated with the liposomes for 5 hours at final molar ratio of 1:22.5, 1:11.25 and 1:5.6 (protein:lipid).

3.12. Structure modelling

Once no structure is available for trypanosomatid NTRs and facing difficulties in crystallizing TcNTR72, molecular modelling techniques were exploited for a better understanding of TcNTR structure. Two homology models for TcNTR were build. One, comprising the residues 72 to 312 (Figure 10) was built at the iTasser server. iTasser searches for PDB templates of structural fragments, further combined to generate the full-length structure model (YANG et al., 2014). Another one used the SWISS-MODEL server (WATERHOUSE et al., 2018), which used the residues 77 to 312, comprising the globular domain. An *ab initio* model was also built with the help of the server Quark (XU; ZHANG, 2012, 2013). Due to the limitations imposed by the server (maximum 200 residues), an *ab initio* model for TcNTR was built for the fragment comprising residue 88 to 287 (Figure 10).

4. Results

4.1. Expression and purification optimization

The family of bacterial nitroreductases share biochemical properties but little identity (ROLDÁN et al., 2008) (Figure 9). In particular, the TcNTR (GenBank accession no. XP_810645) has 312 amino acid residues and the highest identity with an enzyme with determined structure is 30% with the *Thermus thermophilus* NADH oxidase (PDB code: 1NOX/HECHT et al., 1995). When comparing the sequences, the initial part of TcNTR gene, believed to encode a peptide signal addressing the protein to the mitochondrion, is absent in bacteria. The bacterial sequences starts to align at the believed catalytic domain, around the residue 77 of *T. cruzi*. The residues responsible for FMN binding, R88, S90, K92, Q145, E260, G261 and R300 (numbers based on TcNTR) are conserved among the organisms. The region, in TcNTR, comprising the residues 199 to 222 is absent in most bacterial proteins.

Among, tripanosomatids, TcNTR shares approximately 53% identity with *Trypanosoma brucei* enzyme (TbNTR) (GenBank accession no. XP_846343), 43% with *Leishmania major* enzyme (LmNTR) (GenBank accession no. XP_001687543) (VOAK et al., 2013; WILKINSON et al., 2008b). And the region absent in the bacterial enzymes is present in the protozoans sequences with some residues conserved (Figure 10). Unfortunately, none of the tripanosomatids enzymes has their structures determined. In fact, from all the PDB entries for nitroreductase, the only eukaryote enzyme described is from *Saccharomyces cerevisiae* (PDB code: 4URP/SONG et al., 2015).

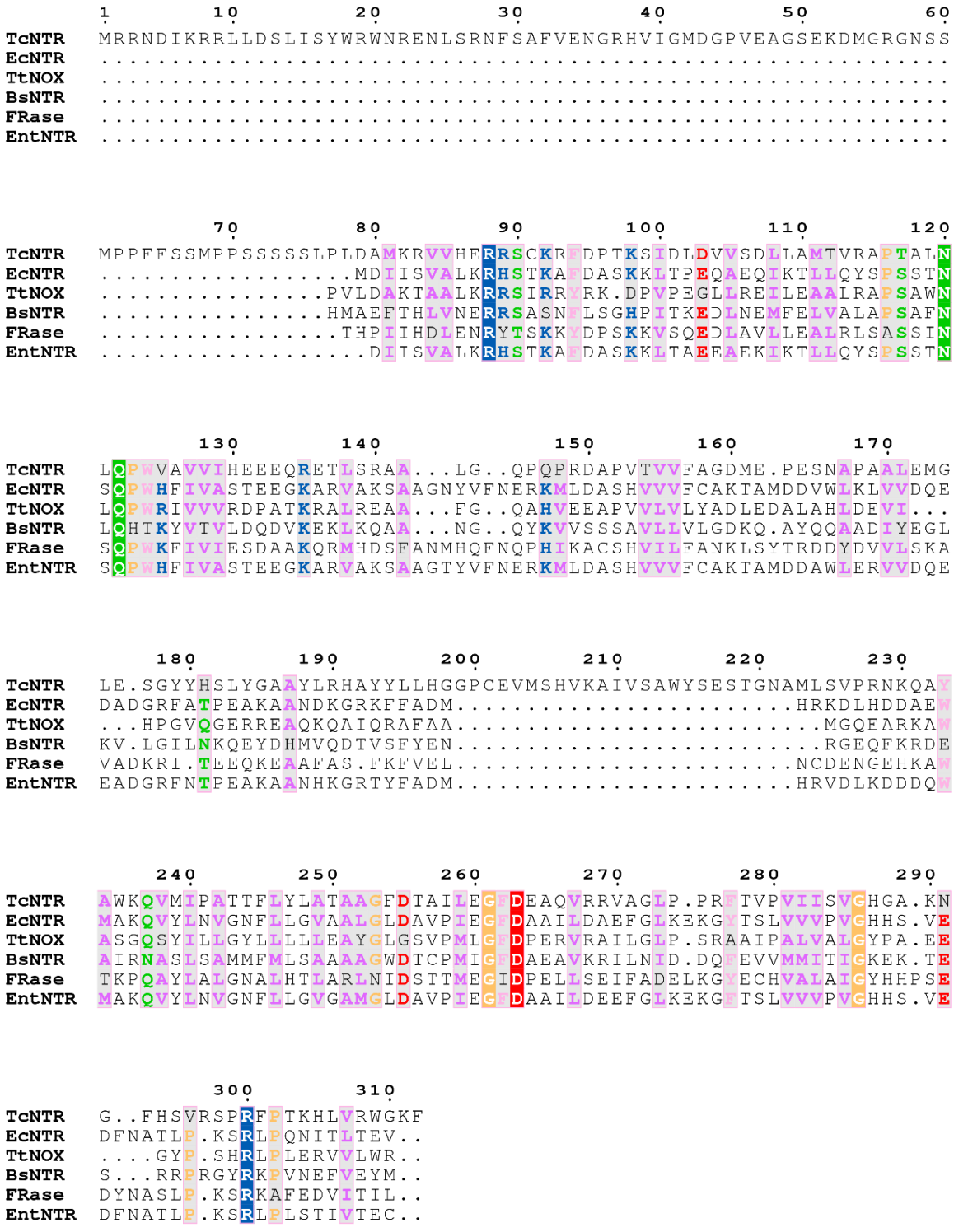

Figure 9: Sequence alignment for nitroreductases from *Trypanosoma cruzi* (TcNTR), *Escherichia coli* (Ec), *Bacilus subtilis* (Bc), *Enterobacter clocae* (Ent), *Thermus thermophilus* NADH oxidase (TtNOX) and NAD(P)H:FMN oxidoreductase from *Vibrio fischeri* (FRase). Similarities in the sequence are highlighted in light gray. The residues were colored by their physicochemical properties: H, K, R – blue, polar and positively charged; D, E – red, polar and negatively charged; S, T, N, Q – green, polar and neutral; F, Y, W – pink, aromatics and non-polar; A, V, L, I, M – purple, aliphatic and non-polar; P, G - orange, small residues; C – yellow, not classified. The alignment was done using the server PROMALS3D (PEI et al., 2008).

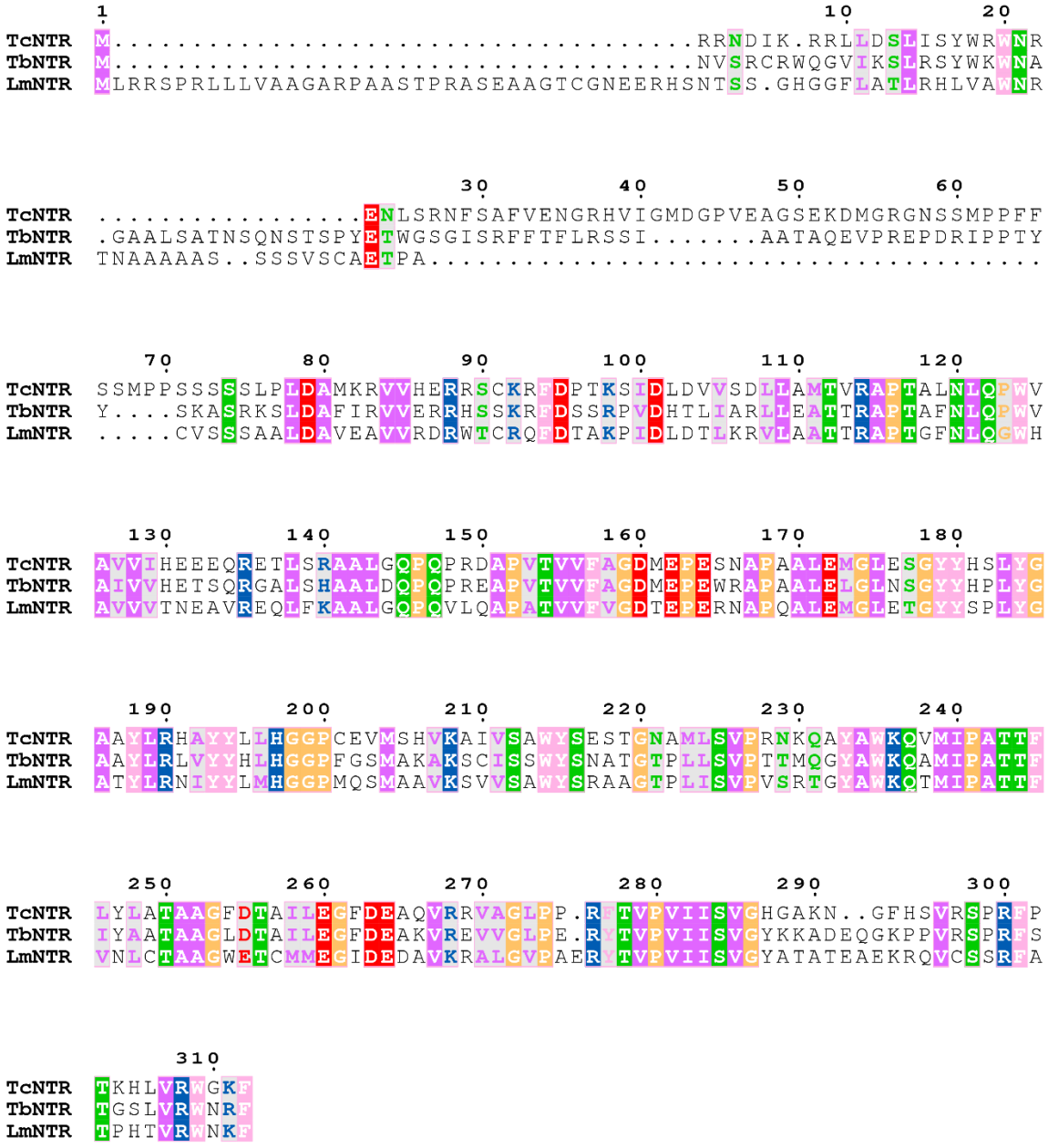

Figure 10: Sequence alignment for nitroreductases from *Trypanosoma cruzi* (TcNTR), *Trypanosoma brucei* (TbNTR) and *Leishmania major* (LmNTR). Similarities in the sequence are highlighted in light gray. The residues were colored by their physicochemical properties: H, K, R – blue, polar and positively charged; D, E – red, polar and negatively charged; S, T, N, Q – green, polar and neutral; F, Y, W – pink, aromatics and non-polar; A, V, L, I, M – purple, aliphatic and non-polar; P, G – orange, small residues; C – yellow, not classified. The alignment was done using the server PROMALS3D (PEI et al., 2008).

Based on a preliminary sequence analysis, NTR can be described as divided in 3 distinct fragments (Figure 11): residues 1 to 14 are predicted to carry a signal peptide, residues 15 to 78 corresponds to an disordered region and residues 78 and further is the protein catalytic domain (WILKINSON et al., 2008b).

Figure 11: Scheme representing the sequence of *Trypanosoma cruzi* nitroreductase type I (Genebank accession no. XP_810645). Secondary structure predicted by JPred4 (Expasy, DROZDETSKIY et al., 2015). Highlighted in red is the putative mitochondrial targeting sequence, in yellow the residues that can be interacting with the prosthetic group FMN and diamonds marks the starting residue of the constructs TcNTR72 and TcNTR78.

During the development of the present project, two different TcNTR fragments were evaluated: TcNTR78 and TcNTR72. The construct TcNTR78, kindly donated by our collaborator Shane Wilkinson from the Queen Mary University of London, has been used as a model for a series of studies performed in his laboratory (BOT et al., 2013; HALL et al., 2010; HALL; BOT; WILKINSON, 2011b; HALL; MEREDITH; WILKINSON, 2012; WILKINSON et al., 2008b). Unfortunately, in our hands, the expression and purification protocol previously reported, resulted in low expression yields and low protein stability.

TcNTR78 expression induced by IPTG yield approximately 1 mg/L of culture. The quantification was performed using the absorbance of the FMN prosthetic group as a probe. The characteristic molar extinction coefficients (ε) for TcNTR was determined and protein concentration was then estimated monitoring the absorbance of protein-bound FMN as described by equation 1. According to the absorption spectra for TcNTR, the maximum absorbance was found at 461 nm (Figure 12, $\varepsilon_{461\,nm}$ [TcNTR78] = 13489 mol^{-1} L cm^{-1}).

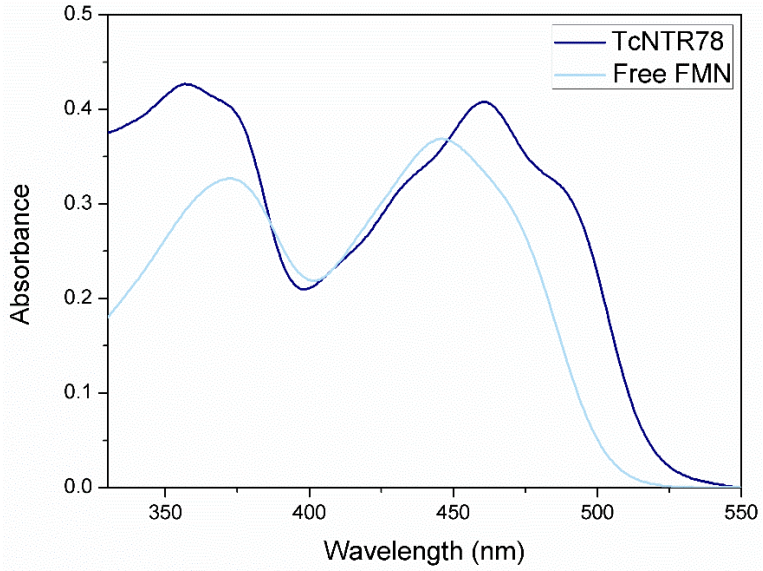

Figure 12: Absorbance spectra of purified TcNTR78 exhibiting a two peaks spectra characteristic flavin profile. Maximum peak was found at 461 nm and used for protein quantification.

SDS-PAGE analysis indicated that TcNTR78 was successfully purified (Figure 13) and isolated TcNTR78 protein was found active (Figure 14). DLS experiments revealed the presence of a single but heterogeneous peak (polydispersity above 20%) compatible with a particle of approximately 9 nm in diameter in average (Figure 15). TcNTR78 displayed high instability under short term storage (overnight at 4°C).

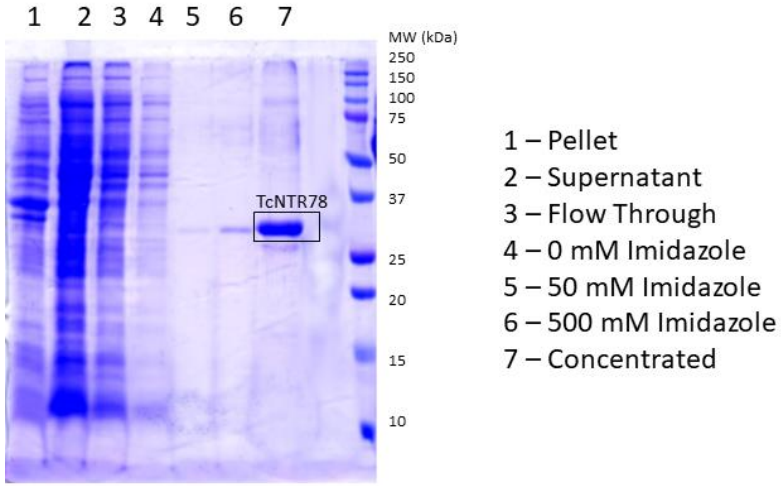

Figure 13: SDS-PAGE analysis of TcNTR78 purification showing the pure protein on lane 6 and 7 with the expected weight of around 30 KDa.

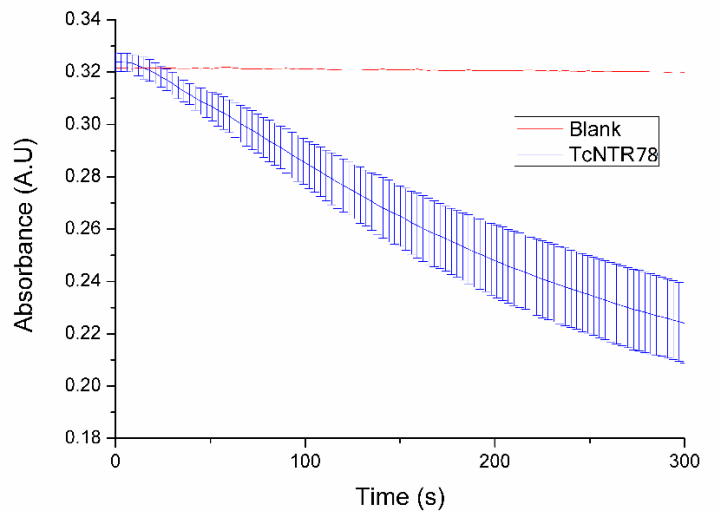

Figure 14: Consumption of NADH by TcNTR78 monitored by absorbance at 340 nm.

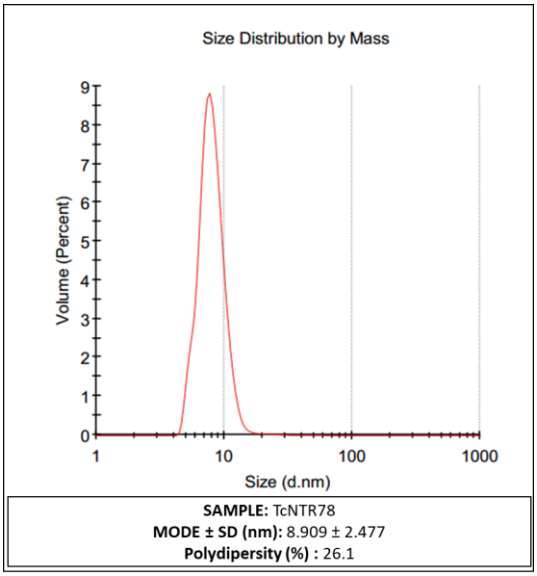

Figure 15 : Dynamic light scattering analysis of TcNTR78 solution showing its hydrodynamic diameter.

In order to optimize protein yield and achieve higher stability several efforts have been made, including changes in the original protocol for protein production. Also, we used *in silico* analysis to explain the lack of stability of TcNTR78. In our studies we found that an α-helix was predicted to start at the residue 78 (Figure 11) (JPred - Expasy, DROZDETSKIY et al., 2015). We speculated that cutting the protein at the very beginning of the first helix, as found in the construct TcNTR78, could cause destabilization of the N-terminal stretch, and be responsible for the observed lack of stability. In order to evaluate our hypothesis, a new construct, TcNTR72, 6 residues longer than TcNTR78, was tested.

For the construct TcNTR72 different bacterial strains and IPTG concentrations were tested (Figure 16). The strain Rosetta (also used for TcNTR78) was chosen due to higher

expression levels of the protein in its soluble form. The temperature of induction and IPTG concentration were further optimized and the condition chosen for TcNTR72 was 300 μM of IPTG and induction at 17ºC. The construct was successfully purified with a yield of 2 mg/L ($\varepsilon_{461\,nm}$[TcNTR72] = 12271 mol^{-1} L cm^{-1}).

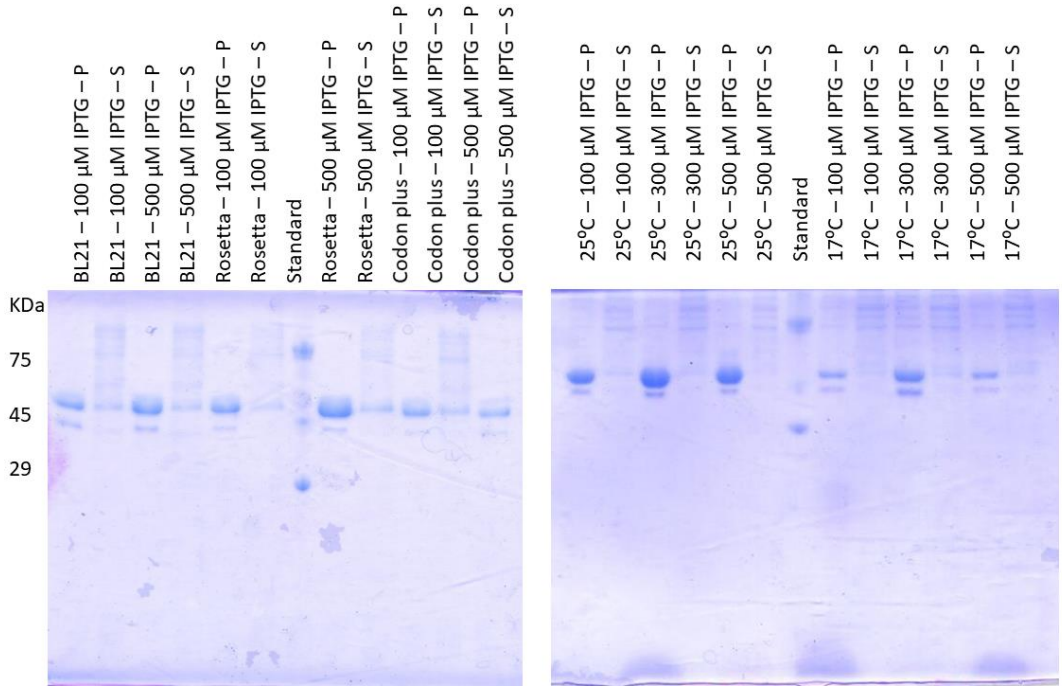

Figure 16: SDS-PAGE analysis for TcNTR78 expression. Soluble and insoluble fractions of cell culture for (a) different bacterial strains after induction at 17ºC with two concentrations of IPTG and (b) the strain Rosetta™ after induction with different concentrations of IPTG with an induction at 25ºC and 17ºC.

In this protocol, the T7 RNA polymerase is under control of a *lacUV5* promoter and the addition of isopropyl-β-D-thiogalactoside (IPTG) triggers transcription of the lac operon. The target protein, under a T7 promoter, will be transcribed and translated at high rate. Aiming at increasing the yield, the construct TcNTR72 was successfully submitted to an autoinduction protocol in which high density cultures are achieved due to the presence of glucose. The pH is controlled by sodium and potassium phosphates, which also provides ions along with the other components. After the depletion of glucose the induction is initiated using glycerol and lactose as carbon sources (STUDIER, 2005). The temperatures of 37 and 20ºC were tested and the cultures were monitored until reaching saturation, which occurred after 48 hours (Figure 17). At 20ºC a higher concentration of soluble protein was observed where the remarkable yield of 18 mg/L of cell culture was obtained. Under similar autoinduction expression conditions, no substantial increase in protein yield was observed for TcNTR78, estimated in 1.5 mg /L of cell culture.

SDS-PAGE analysis indicated that TcNTR72 was successfully purified (Figure 18). And the isolated protein was found active (Figure 19). DLS experiments also revealed the presence of a single but heterogeneous peak (polydispersity above 20%) compatible with a particle of approximately 9 nm in diameter in average (Figure 21), similar to values obtained to TcNTR78 protein.

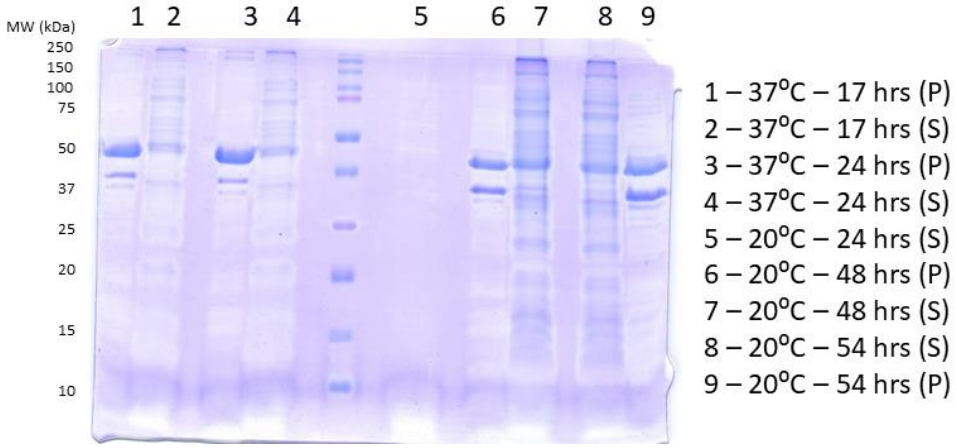

Figure 17 : SDS-PAGE analysis for TcNTR72 expression. Soluble (S, supernatant) and insoluble (P, pellet) fractions of cell culture showing the difference in autoinducted protein production with time and temperature using the bacterial strain Rosetta™.

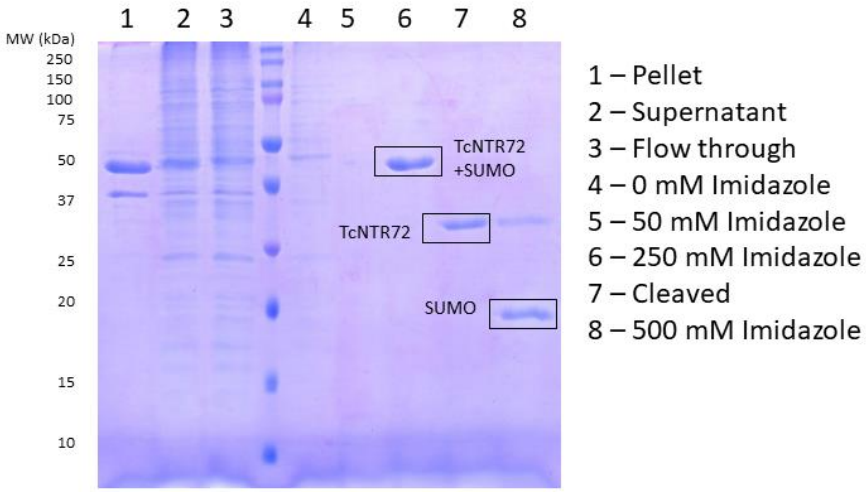

Figure 18: SDS-PAGE analysis of TcNTR72 purification. The pure and tag free protein is showed in lane 7.

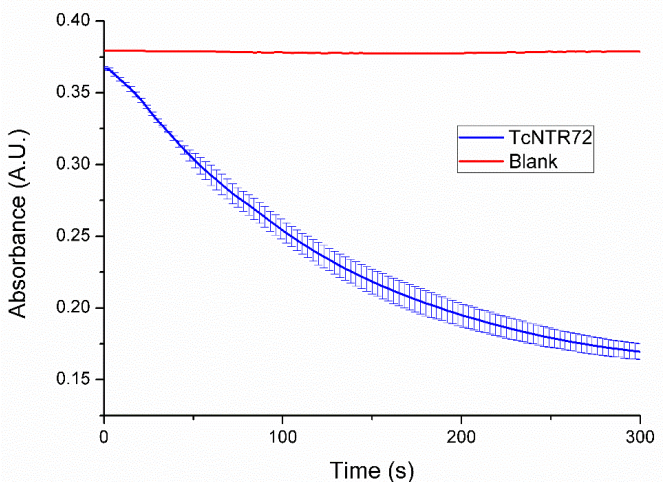

Figure 19: Consumption of NADH by TcNTR72 monitored by absorbance at 340 nm.

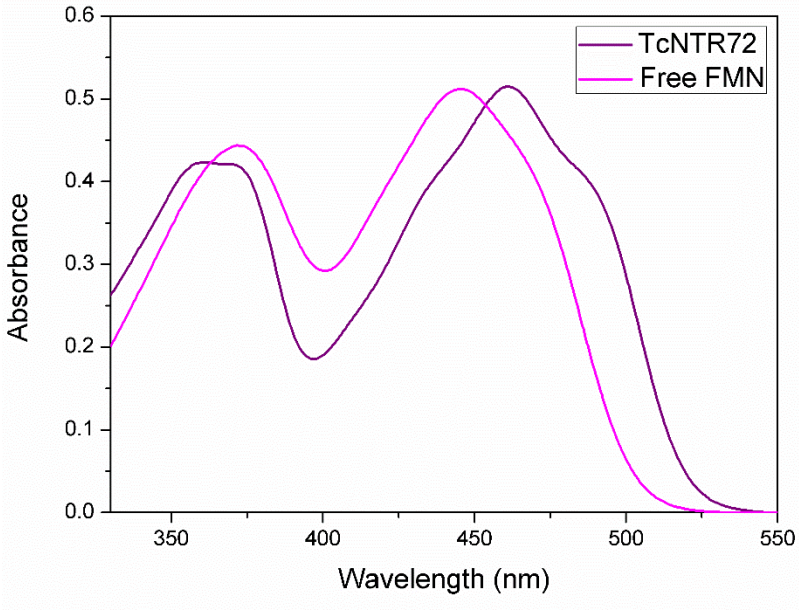

Figure 20: Absorbance spectra of construct TcNTR72 also exhibiting a maximum peak at 461 nm.

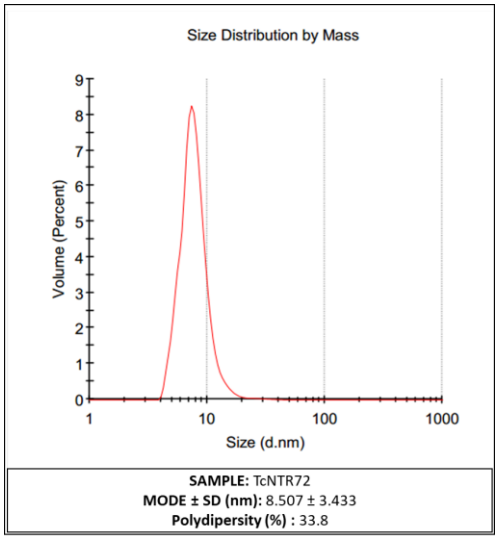

Figure 21: Size distribution of TcNTR72 solution obtained from DLS.

SYPRO-orange, commonly used as a probe to monitor protein denaturation in DSF experiments as well as other hydrophobic fluorophores, gives rise to a fluorescence signal when binding to exposed hydrophobic areas of unfolded proteins. Hence, due to the presence of detergent in our protein samples, the SYPRO-orange was found incompatible. FMN was then chosen as a probe to monitor thermal stability. Our preliminary fluorescence studies performed by ThermoFMN reveals a high initial background signal and a small increase in fluorescence intensity when comparing native and denatured state (Figure 22). Those findings suggest that the FMN flavin group could be found solvent exposed. Our findings are in agreement with structural data available for other NTRs including the ones from *Thermus thermophilus* and *Escherichia coli,* in which the prosthetic group is tightly bound but sits in a shallow pocket located in the protein surface (Figure 23)(HECHT et al., 1995; PARKINSON; SKELLY; NEIDLE, 2000).

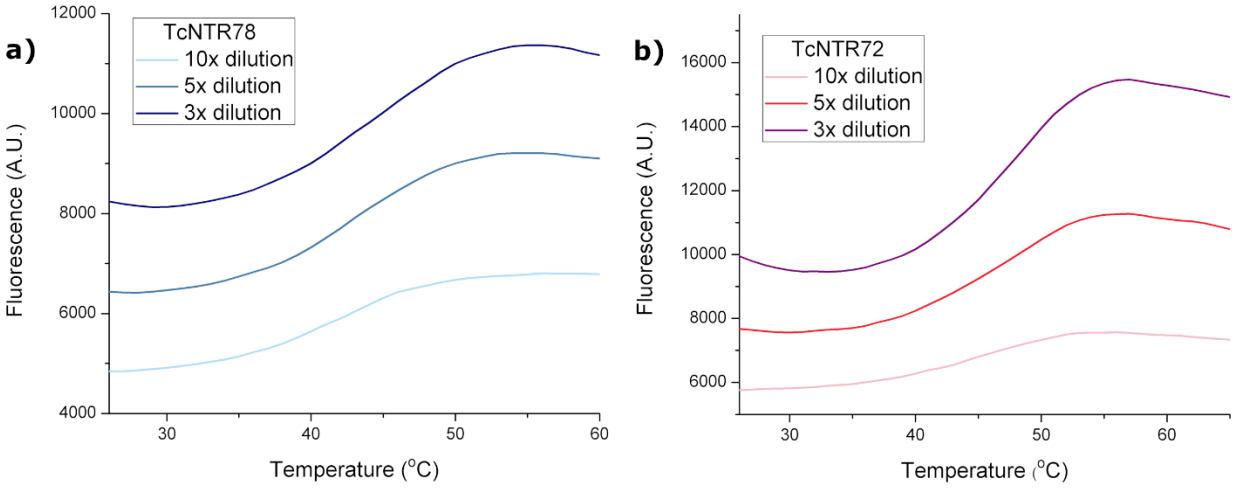

Figure 22 : Melting curves for both constructs monitored by the fluorescence of the FMN prosthetic group in presence of water. The sigmoidal fitting against the data was used to determine the melting temperatures found as 41 ºC, 48 ºC for TcNTR78 and TcNTR72, respectively.

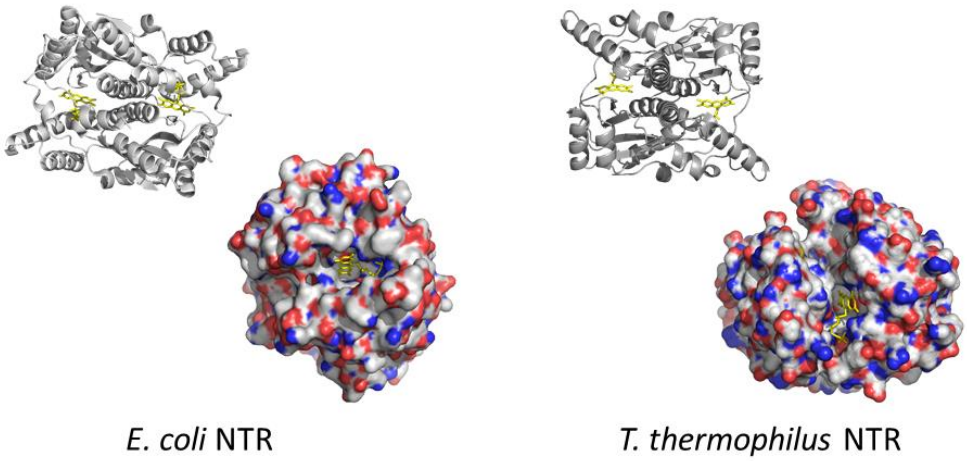

Figure 23 : Nitroreductase from *Escherichia coli* (PDB code: 1DS7) and *Thermus thermophilus* NADH oxidase (PDB code: 1NOX) in both cartoon and surface representation showing the solvent exposed flavin.

Denaturing curves for both constructs were undertaken and compared. TcNTR72 was shown to be more stable (Figure 24), due to a higher melting temperature and a steeper curve, evidence of a cooperative unfolding. The difference in Tm, and lower thermal stability of TcNTR78 can be explained by either the predicted misfolding of the first helix or due to the presence of the His-tag in TcNTR78 (BOIVIN; KOZAK; MEIJERS, 2013).

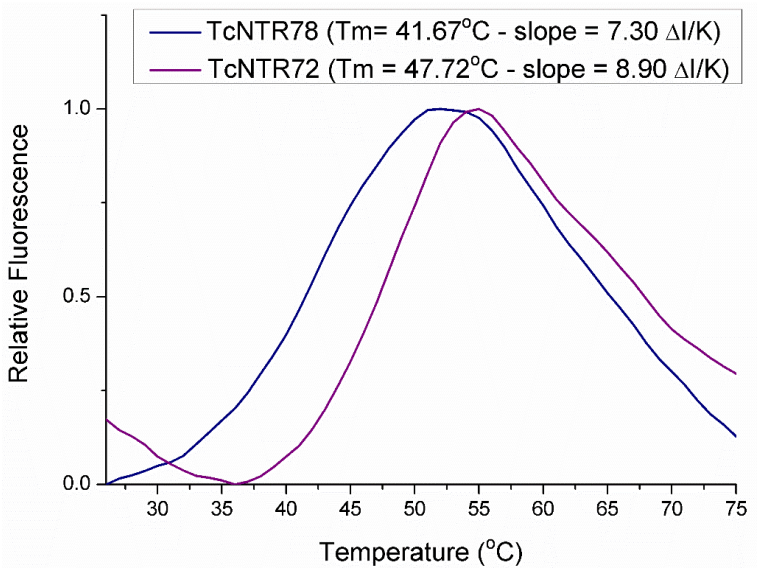

Figure 24 : Comparison of the melting temperatures of constructs TcNTR78 and 72 by ThermoFMN.

Aiming at maximizing protein stability and homogeneity crucial to achieve protein crystallization and allow structural studies, different physicochemical conditions were evaluated by DSF and DLS experiments.

Initially, the influence of sodium chloride on protein unfolding was investigated by ThermoFMN under a broad range of pHs and buffers using the Hampton Solubility and Stability 2 kit (Figure 25). No clear transition curves were observed under acidic pHs possible due to

destabilization of both constructs. At the pH 7, 7.5 and 8.5 there is possible interference of the buffering agent (imidazole, hepes and bis-tris propane, respectively) in the distortion of the melting curve, since different substances at the same pH does not have this effect. For both constructs the increase in sodium chloride concentration had a negative effect on the protein stability, decreasing the melting temperature or inducing a loss of the typical denaturing curves.

ThermoFMN TcNTR78 – Tm = 41.67°C

ΔTm / NaCl (mM)	**Sodium Acetate** pH 4.5	**Sodium Citrate** pH 5	**Succinic Acid** pH 5.5	**MES** pH 6	**BIS-TRIS propane** pH 6.5	**Imidazole** pH 7	**HEPES** pH7.5	**TRIS** pH 8	**BIS-TRIS propane** pH 8.5	**AMPD** pH 9	**Glicine** pH 9.5
0	-	-	-	-	-	-	-2.0	1.5	-	-0.3	3.3
50	-	-	-	-	-	-	*	0.9	-	0.7	3.1
100	-	-	-	-	-	-	-	3.5	-	3.2	3.3
150	-	-	-	-	-	-	-1.4	3.5	-	-	3.2
200	-	-	-	-	-	-	-0.4	-	-	-	-
250	-	-	-	-	-	-	-	-	-	-	-
500	-	0.5	-	-	-	-	-	-	-	-	-
1000	-	-	-	-	-	-	-	-	-	-	-

ThermoFMN TcNTR72 – Tm = 47,72°C

ΔTM / NaCl (mM)	**Sodium Acetate** pH 4.5	**Sodium Citrate** pH 5	**Succinic Acid** pH 5.5	**MES** pH 6	**BIS-TRIS propane** pH 6.5	**Imidazole** pH 7	**HEPES** pH7.5	**TRIS** pH 8	**BIS-TRIS propane** pH 8.5	**AMPD** pH 9	**Glicine** pH 9.5
0	-	-	-	-	-	-	-	-3.0	-	-2.9	-0.5
50	-	-	-	-	-	-	-	-2.6	-	-3.5	-1.0
100	-	-	-	-	-	-	-	-4.4	-	-3.9	-3.4
150	-	-	-	-	-	-	-	-	-	-4.3	-3.7
200	-	-	-	-	-	-	-	-	-	-5.1	-4.4
250	-	-	-	-	-	-	-	-	-	-5.2	-5.5
500	-	-	-	-	-	-	-	-	-	-	-9.7
1000	-	-	-	-	-	-	-	-	-	-	-

Figure 25 : Difference in Tm values of both constructs under different buffer conditions. The gray cells indicates no clear transition observed. A negative ΔTm higher than 2 °C is showed in red, in yellow the difference is lower than ±2°C and in green the ΔTm is higher than 2°C. * Multi-phasic unfolding.

Considering that low salt concentration is usually required for the success of protein crystallization and considering that DSF suggests an increase in stability at lower salt concentrations, we investigated, on TcNTR72, the minimum amount of sodium chloride necessary to avoid aggregation and promote protein stability (Figure 26 and 27). Protein solution containing 100 to 300 mM of sodium chloride presented similar values of melting temperature while at 500 mM the curve was distorted. At the NaCl concentration of 400 mM, the protein solution had the highest melting temperature but presented polydisperse. In DLS, only the solutions with 100 and 300 mM were homogeneous. Based on both ThermoFMN and DLS experiments, and considering that at the salt concentration of 100 mM the enzyme tends to precipitate under short term storage (1-2 hours), 300 mM of salt was identified as the minimum salt concentration required to promote protein stabilization. Compared to the initial 500 mM used in the elution buffer, reduction of salt concentration to 300 mM of sodium chloride was found to increase the melting temperature of both constructs and to reduce sample dispersity of TcNTR72 (Figure 28).

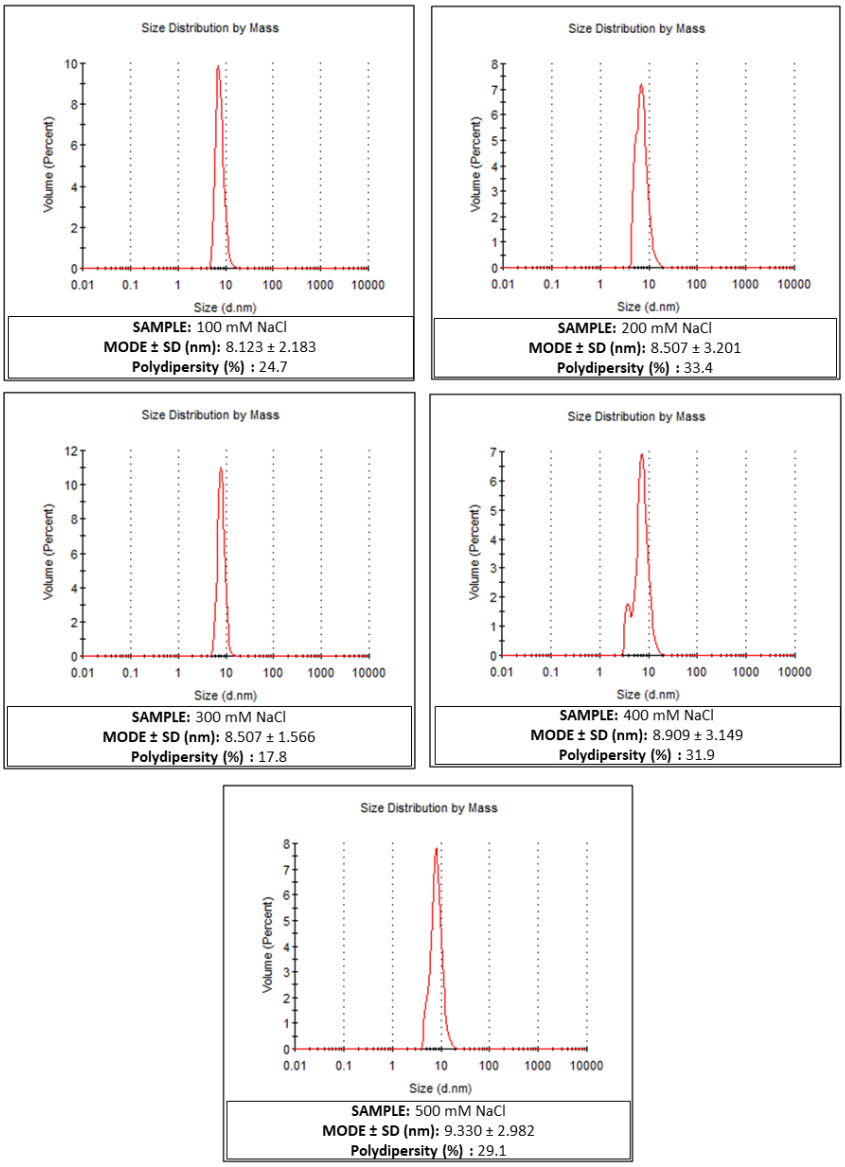

Figure 26: Size distribution of TcNTR72 solution obtained from DLS Analysis of the different sodium chloride concentrations versus the size distribution.

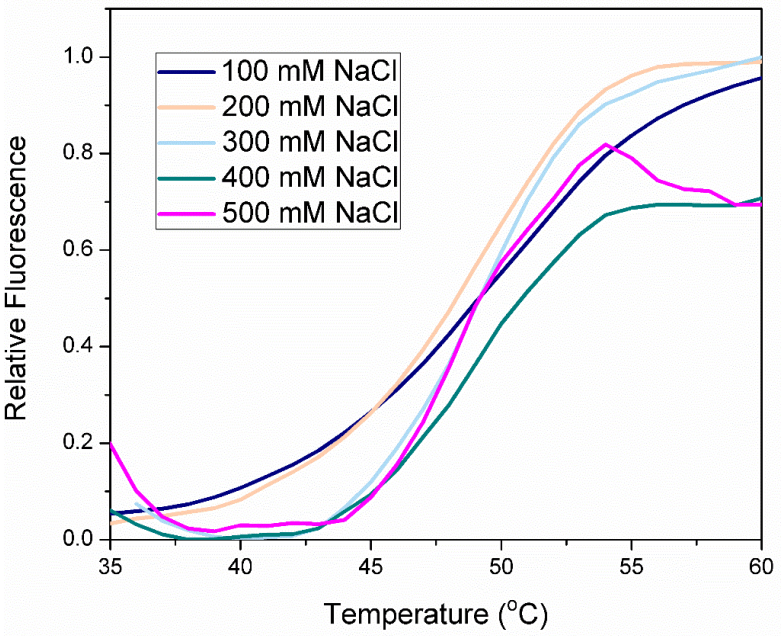

Figure 27 : Influence of different sodium chloride concentrations on the melting temperature of the construct TcNTR72.

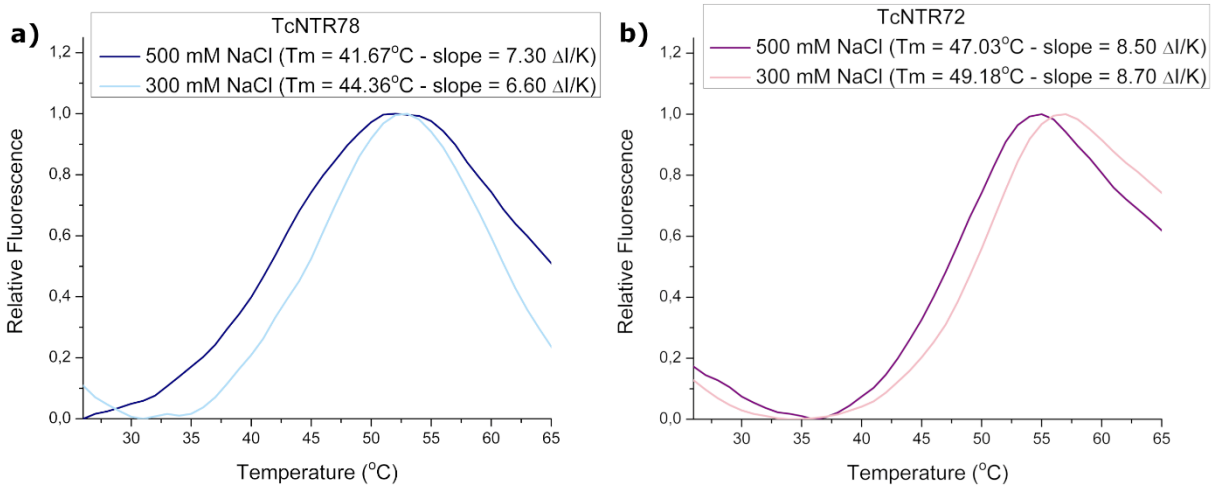

Figure 28 : Evaluation of the influence of sodium chloride concentration used in the purification buffer on TcNTR78 (a) and TcNTR72 (b) melting temperatures.

The influence of additives in enhancing protein stability were also evaluated using Hampton Solubility and Stability 1 kit. The variation in ΔTm values obtained for the two different constructs with the same additive could be explained as due to different Triton X-100 concentrations (since the purification procedure vary from one construct to the other) or due to structural changes (especially the presence of a his-tag in construct TcNTR78 which could block some interaction sites) (Table 2).

We highlight the effect promoted by betaine monohydrate, a zwitterion, which stabilized both constructs (Figure 29). For TcNTR72 construct, a positive shift in Tm was also achieved

in the presence of non-aromatic non-detergent sulfobetaines (NDSB 195, 211 and 221) while in TcNTR78 no significant changes were observed. On the other hand, the sulphonated derivatives possessing aromatic rings (compounds NDSB 201 and 256) had a negative influence on both constructs by decreasing the melting temperature or not showing the transition. One explanation for the quenching of the fluorescence phenomema for these compounds could be due to a direct interaction with the prosthetic group FMN. Another highlight is cholin, present in the phospholipids head groups also stabilize both constructs.

Table 2: Additives with a positive shift above 3ºC in at least one construct. Reference values: TcNTR72 – Tm = 47.20 ºC/slope = 7.1 ΔI/K; TcNTR78 – Tm = 44.36ºC/slope = 6.6 ΔI/K.

Component	**[ ] mM**	**TcNTR72**		**TcNTR78**	
		ΔTm (ºC)	**Slope (ΔI/K)**	**ΔTm (ºC)**	**Slope (ΔI/K)**
D-(+)-Trehalose dehydrate	375	2.99	7.7	2.81	6.8
Xylitol	1000	3.48	8.1	1.04	7.2
D-Sorbitol	1000	3.94	8.9	1.14	7.4
Sucrose	1000	-	-	3.51	5.8
Triethylene glycol	5%	3.5	13.4	-0.68	7.5
GSH (L-Glutathione reduced)/ GSSG (L-Glutathione oxidized)	20/20	6.11	40.6	-	-
Betaine monohydrate	1250	6.14	7	3.71	10.1
Non Detergent Sulfobetaine 195 (NDSB-195)	500	3.51	10.1	-0.05	4.8
Non Detergent Sulfobetaine 201 (NDSB-201)	500	-	-	-	-
Non Detergent Sulfobetaine 211 (NDSB-211)	500	3.88	9.2	1.43	5.9
Non Detergent Sulfobetaine 221 (NDSB-221)	500	3.36	9.3	0.9	6.4
Non Detergent Sulfobetaine 256 (NDSB-256)	400	-1.93	7.6	-1.77	5.5
Cholin acetate	12.5%	1.77	12.6	3.8	17.4
Glycerol	25%	4.21	7.9	5.78	6.4
(2-Hydroxypropyl)-β-cyclodextrin	5	3.78	5.6	-2.28	7.2

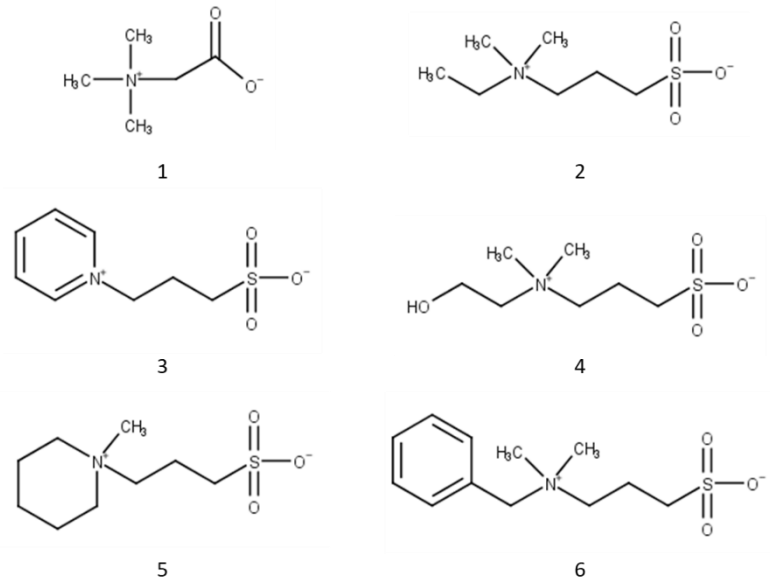

Figure 29 : Chemical structure of betaine and its non-detergent sulfonated derivatives: (1) betaine; (2) non detergent sulfobetaine 195/NDSB-195; (3) non-detergent sulfobetaine 201/NDSB-201; (3) non-detergent sulfobetaine 211/NDSB-211; (4) non-detergent sulfobetaine 221/NDSB-221; non detergent sulfobetaine 256/NDSB-256.

Glycerol in a concentration of 25% was found to induce a positive Tm shift for both constructs (Table 2). Thus, the addition of 10% of glycerol during purification was used as a strategy to increase the stability of TcNTR72 enzyme. No significant changes were observed in the thermal stability or homogeneity of TcNTR72 solution in presence of glicerol at a concentration appropriate for use in the purification buffer. This way, glycerol was not used as an additive in further experiments (Figure 30).

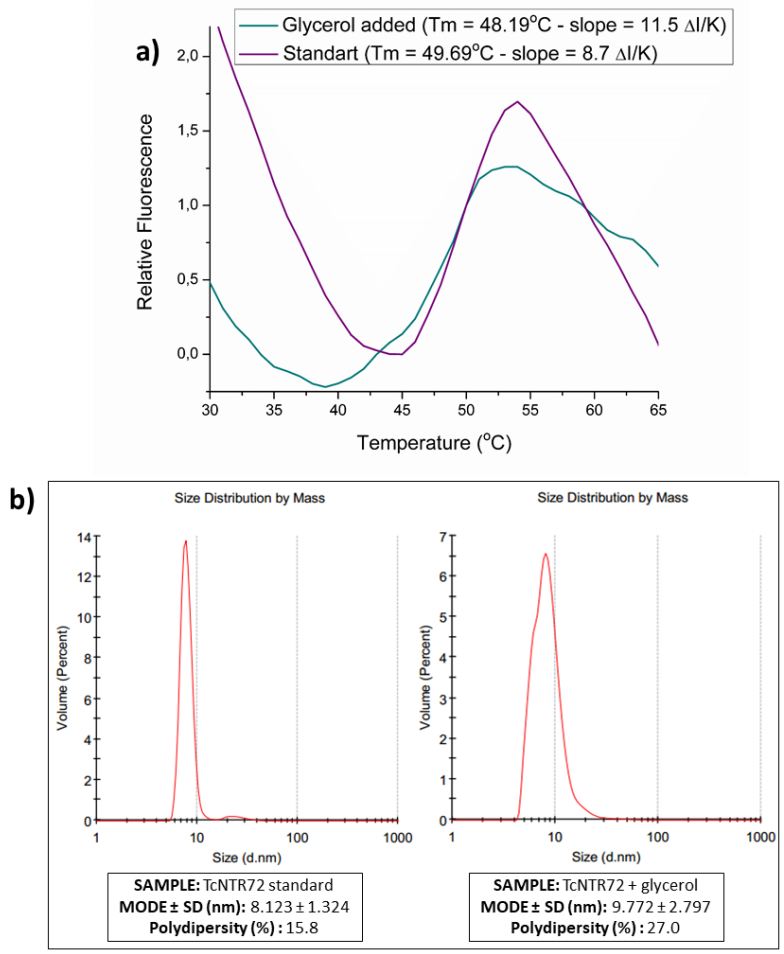

Figure 30: Analysis by ThermoFMN and DLS of the construct TcNTR72 purified with the addition of 10% of glycerol. No significant contribution was observed in terms of protein stability and homogeneity.

In order to evaluate the relevance of Triton X-100 for protein stability, a purification protocol in absence of the detergent was designed and tested. Protein purity was assessed by SDS-PAGE (Figure 31). Curiously the lack of the characteristic yellow color in the protein (absorbance at 461 nm= 0.03) and the increase in hydrodynamic diameter (Figure 30), suggest that the detergent is essential for purification of TcNTR72 by preventing aggregation of protein particles and protecting TcNTR72 from losing the prosthetic group FMN. In addition, only a residual activity was observed for the detergent free purified protein, as expected due to the loss of FMN. This loss of the prosthetic group indicates that the detergent is necessary to stabilize this region of interaction.

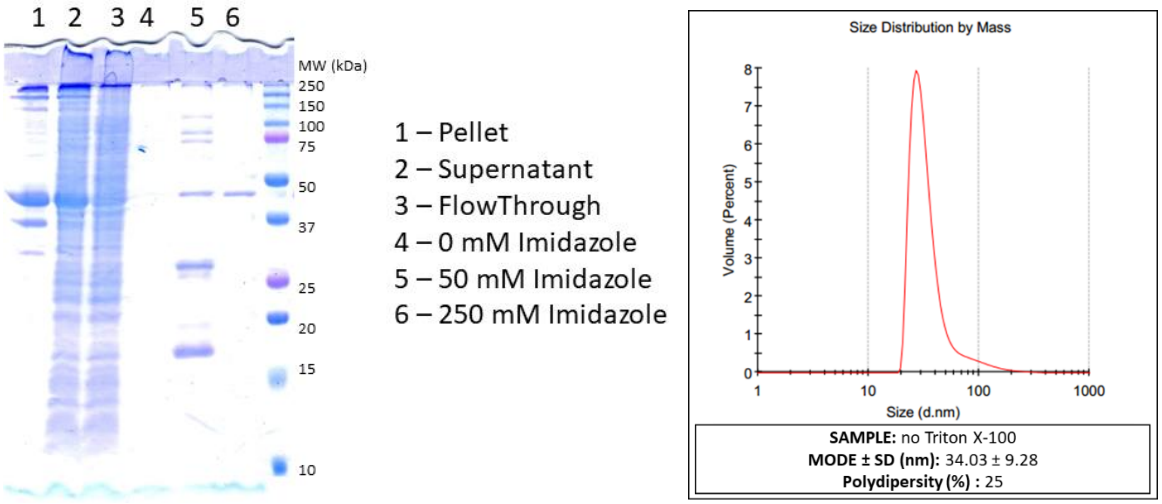

Figure 31: SDS-page showing the purification of TcNTR72 without Triton X-100, in lane 6 we can observe the protein with the SUMO tag attached (approximately 42 kDa). Size distribution of the tag-free TcNTR72 after purification without the detergent.

Due to the positive effect of Triton X-100 on protein stability, we decided to investigate the impact of other detergents on both TcNTR72 and TcNTR78. Protein stability in presence of different detergents [Detergent Screen (Hampton Research)] was assessed by ThermoFMN (PÁDUA et al., 2014). Several detergents were found to stabilize TcNTRs and the best results are found summarized in table 3. But, as the additives, we did not observe a consistency between the constructs and the detergents CHAPS, n-Octyl-β-D-thiomaltoside, Cymal 2 and 6 had a positive effect only in one of them. Some of the Anapoe detergents are the ones that promotes a stabilization on TcNTR72 and 78, curiously, they have the same chemical formula as the Triton series but possess less peroxide, which can interfere with protein folding (WEIDS et al., 2016).

Table 3: Detergents that presented a positive influence in the protein thermal stability, both constructs in comparison. Reference values: TcNTR72 - Tm = 44.0ºC/slope = 7.0 ΔI/K; TcNTR78 – Tm = 41.32ºC/slope = 6.0 ΔI/K. Differences between both constructs as well as some degree of lack of reproducibility in the Tm was observed and could be explained as a results of differences in the final Triton X-100 concentration for each batch of purification.

Detergent	**TcNTR72**		**TcNTR78**	
	ΔTm (ºC)	**Slope (ΔI/K)**	**ΔTm (ºC)**	**Slope (ΔI/K)**
Anapoe 58	3.19	6.8	2.04	7.8
Anapoe X-114	2.22	6.2	3.29	10.5
Anapoe X-405	3.94	8.6	3.47	9.3

CHAPS	2.96	3.7	0.7	6.6
n-Octyl-β-D-thiomaltoside	-0.27	11.2	4.86	30.9
Cymal-6	3.67	5.3	0.5	6.3
Cymal-2	-	-	8.94	41.8

The fact that detergents were observed to keep structural integrity, thermal stability, and activity of TcNTR, prompted to us the idea of investigating the presence of hydrophobic patches in the protein, as well as, their potential function. As a first step towards this goal, a potential protein-lipid interaction was investigated by calorimetric studies.

4.2. Analysis of membrane interaction

DPPC was chosen as a model of study for studying the protein-lipid interaction. Liposomes made of DPPC were initially incubated with TcNTR in different incubation periods at the molar ratio of 1:90000 and the protein solution contained about 1% of Triton X-100. DSC measurements were carried out and thermograms were recorded (Figure 32 and Table 4).

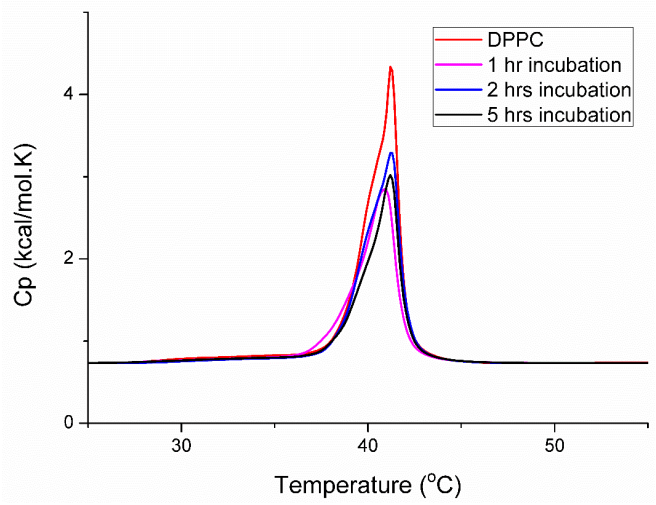

Figure 32: DSC Thermogram. Effect of incubation time between DPPC liposomes and TcNTR on the lipid phase transition. Proportion of 1: 90000 in mols of protein: lipid was used.

Table 4: Thermodynamic parameters obtained by DSC and size evaluation of liposome samples by DLS for DPPC liposomes and the effect of the different incubation time with TcNTR.

DPPC-Liposomes	Diameter (nm)	Polydispers. Index	ΔH (kcal/mol)	ΔS (kcal/mol.K)	T_c (°C)	$t_{1/2}$
Liposomes	152 ± 2	0.013	9.52	0.0303	41.3	2.00
1h incubation	151 ± 2	0.029	6.29	0.0200	40.9	2.12
2h incubation	145 ± 2	0.058	6.51	0.0207	41.3	2.00
5h incubation	148 ± 1	0.006	5.71	0.0182	41.2	1.85

No significant changes are observed in the size and polydispersitivity of the liposomes, considering the DLS sensitivity. In the thermodynamics parameters the most significant change is observed in the enthalpy values of the lipid phase transition (ΔH) , a variation that increases along with the incubation time. And aiming to maximize the effect of incubation with the protein, 5 hours was the time chosen.

In order to avoid Triton X-100 interference, the detergent was then removed from TcNTR sample by adsorption, using the Calbiosorb resin. DPPC liposomes were then incubated with the TcNTR enzyme, after removal of the detergent. A 0.8 μm Millipore filter was used for removing aggregates formed with the detergen removal. The molar ratio of 1:90000 (protein: lipid), lipid concentration and buffer kept unchanged. Based on previous results, incubation time was set to 5 hours. DSC measurements were carried out for filtered and unfiltered samples and thermograms were recorded (Figure 33 and Table 5). The decrease in the enthalpy of transition is also observed indicating that the effect seen previously was not due to the presence of the detergent Triton X-100. The transition peak was also larger ($t_{1/2}$, width at half the peak high, is higher), indicating a less cooperative transition. Regarding the filtered sample, the variation in the enthalpy and the $t_{1/2}$ is smaller than the unfiltered sample.

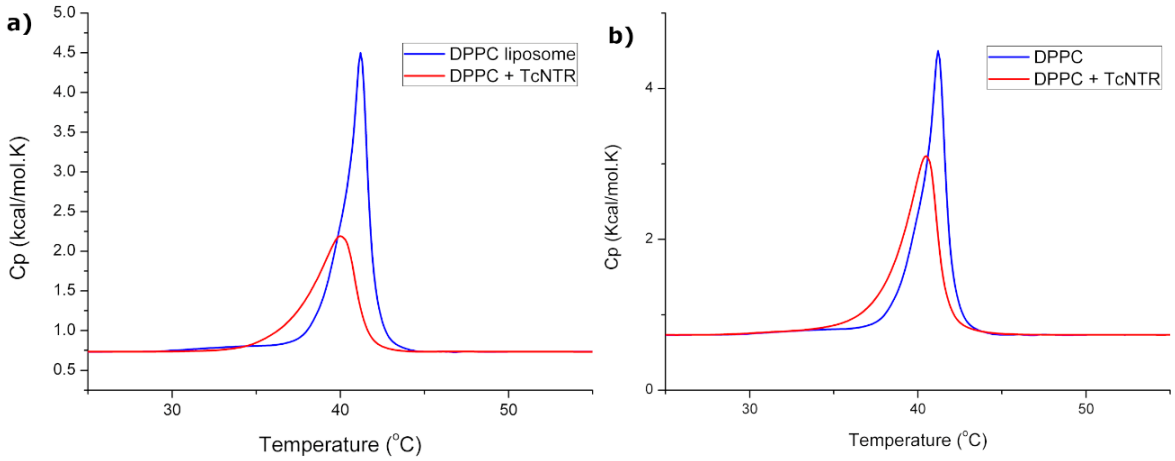

Figure 33: Effect of incubation on the thermal transition of DPPC liposomes with the construct TcNTR72 free of detergent (a) and filtered (b) in the proportion of 1: 90000 in mols of protein: lipid obtained by DSC.

Table 5: Thermodynamic parameters obtained by DSC and size evaluation of liposome samples by DLS for DPPC liposomes and the effect of incubation for 5 hours with TcNTR protein after removal of Triton X-100 detergent and after removal of the aggregates by filtering with 0.8 μm filter.

	DPPC Liposomes	**DPPC + TcNTR**	**DPPC + TcNTR filtered**
Diameter (nm)	139 ± 1	144 ± 1	146 ± 2
Polidipersitivity	0.022	0.035	0.019
ΔH (kcal/mol)	7.9 ± 0.2	5.3 ± 0.4	6.9 ± 0.2
ΔS (kcal/mol.K)	0.0253 ± 0.0006	0.0169 ± 0.0013	0.0222 ± 0.0005
Tc (ºC)	41.1 ± 0.2	39.9 ± 0.3	40.4 ± 0.2
t½	1.4 ± 0.1	2.7 ± 0.1	2.20

In an attempt to verify the presence of the protein in the liposomes, a polyacrylamide gel electrophoresis was performed in which the liposome (supernatant and proteoliposome) samples were treated with hexane for lipid removal (1:1 v/v ratio). The aqueous phase was treated with b-mercaptoethanol and sodium dodecyl sulfate for denaturation. After staining by silver nitrate, no bands related to protein was observed in the liposome samples (Figure 34). However, the presence of the small ubiquitin-like modifier (SUMO) tag was found to be greater than the TcNTR72 in the filtered sample. Therefore, the protein:lipid ratio used in the DSC was not conserved for the filtered sample because, as the quantification was nonspecific, the SUMO tag corresponded to the majority of the sample, what explain the smaller variations observed.

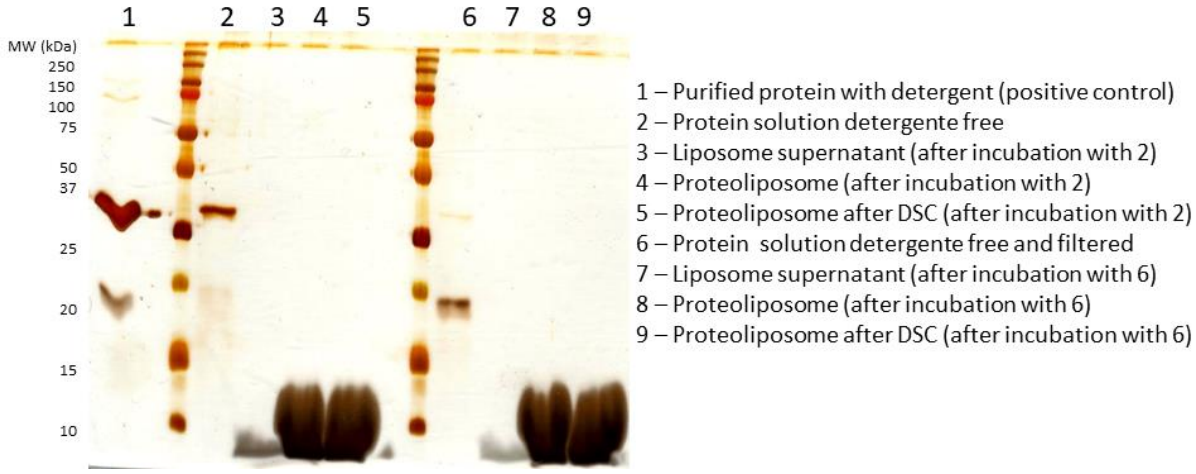

Figure 34: Silver nitrate stained polyacrylamide gel electrophoresis (SDS-PAGE).

In order to verify the interference of the SUMO in the analysis of DPPC liposomes phase transition thermodynamic parameters, the tag was isolated (0.2 mg/mL) and incubated for 5 hours at a molar ratio of 1:90000 (protein: lipid) using the same buffer as TcNTR (50 mM Tris pH 8.5 and 300 mM NaCl). The results (Figure 35 and Table 6) show a small variation in the transition enthalpy which could indicate an interaction between the SUMO tag and the DPPC liposomes. However, this interaction is much smaller than that observed with the TcNTR72, which causes a higher modification in the thermodynamic parameters of the lipid transition. Therefore, the SUMO tag did not influenced the previous results.

Table 6: Thermodynamic parameters obtained by DSC and size evaluation of liposome samples by DLS for DPPC liposomes and the effect of incubation with SUMO tag protein.

	DPPC Liposomes	**DPPC + SUMO**
Diameter (nm)	148 ± 1	143 ± 1
Polidisp. Index	0.087	0.077
ΔH (kcal/mol)	7.7 ± 0.2	7.0 ± 0.3
ΔS (kcal/mol.K)	0.0246 ± 0.0006	0.0222 ± 0.0013
Tc (ºC)	41.2 ± 0.2	41.1 ± 0.2
t½	1.83	1.60

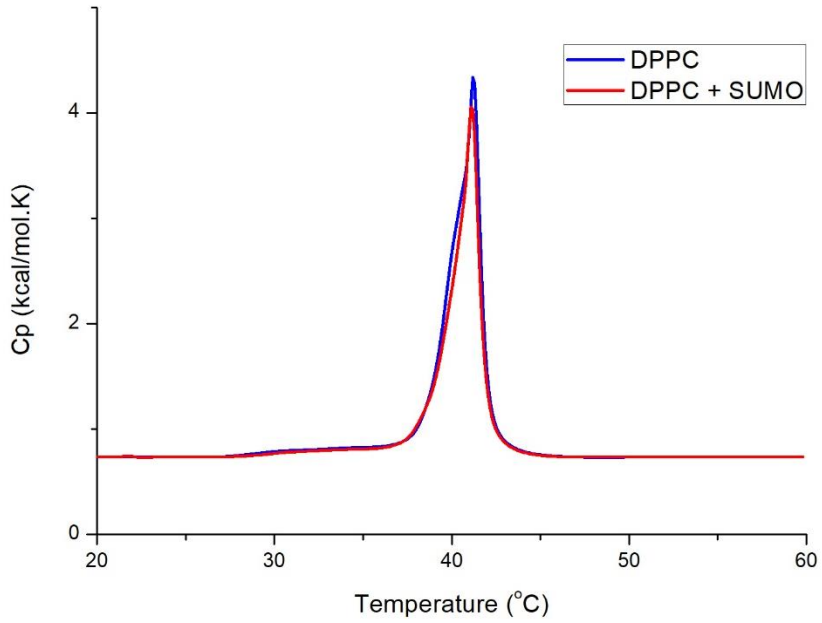

Figure 35: Effect of incubation for 5 hours with SUMO tag protein on the phase transition peak of DPPC liposomes.

The effect of protein:lipid molar ratio and longer incubation periods (Table 7 and figure 36) on the lipid phase transition was verified. The detergent-free TcNTR72 protein was chosen for those experiments. No significant differences in the enthalpy of transition were observed with increasing TcNTR72 protein concentration (ratio 1: 45000) or longer incubation time (22 hours) when compared with the previously obtained data (Figure 33, Table 5), although the increase in the $t_{1/2}$ is no longer observed.

The observation of a decrease in the transition enthalpy without a significant change in the lipid transition temperature (Figure 36 and Table 7), suggests that NTR interacts with DPPC without inducing any major rearrangement in the lipophilic part of the phospholipid, probably by interacting with the polar head composed by phosphocholine (DEMETZOS, 2008). Interesting, those results are in agreement with our previous ThermoFMN data (Table 2) where choline acetate was found to promote a shift in the melting temperature of both constructs.

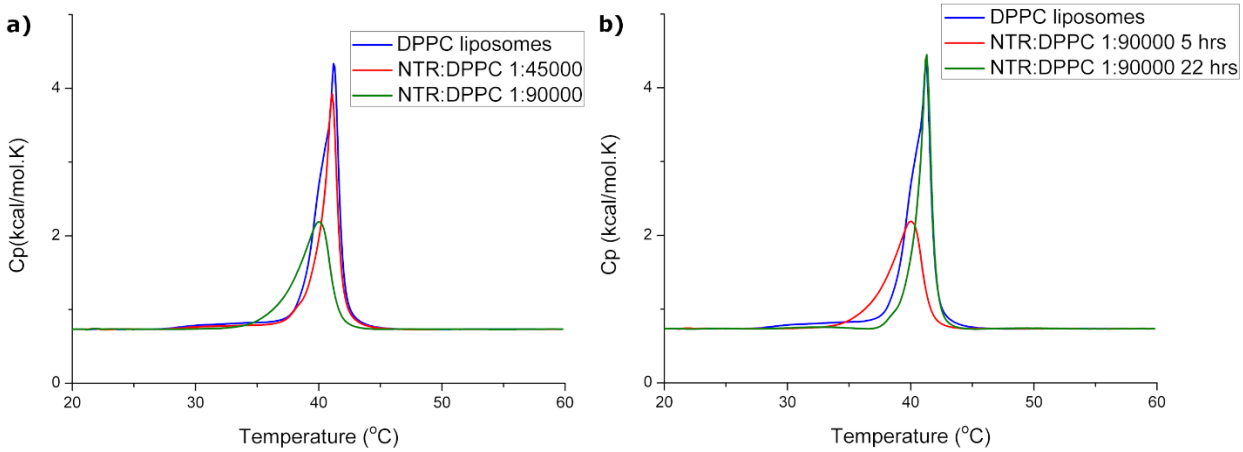

Figure 36: DPPC liposomes thermograms and the effect of incubation with the TcNTR protein in different ratios and at different incubation times, as verified by DSC.

Table 7: Thermodynamic parameters obtained by DSC and size evaluation of liposome samples by DLS for DPPC liposomes and the effect of TcNTR in different proportions and incubation time.

	DPPC Liposomes	**DPPC + NTR (1:90000/5hrs)**	**DPPC + NTR (1:45000/5hrs)**	**DPPC + NTR (1:90000/22 hrs)**
Diameter (nm)	148 ± 2	144 ± 1	141 ± 1	150 ± 4
Polidisp. Index	0.087	0.035	0.094	0.109
ΔH (kcal/mol)	7.7 ± 0.2	5.3 ± 0.4	5.9 ± 0.2	6.9 ± 0.4
ΔS (kcal/mol.K)	0.0246 ± 0.0006	0.0169 ± 0.0013	0.0190 ± 0.0065	0.0190 ± 0.0012
Tc (ºC)	41.2 ± 0.2	39.9 ± 0.3	41.1 ± 0.2	41.3 ± 0.2
t½	1.7 ± 0.1	2.7 ± 0.1	1.4 ± 0.1	1.2 ± 0.1

TcNTR was described to be located in the mitochondrion (WILKINSON et al., 2008). Thus, model membranes where the lipid compositions resembles the one from the inner membrane of this organelle, and contain DPPE and CL lipids were chosen for our sudies. The compositions DPPC: DPPE (3: 1), DPPC: CL (3: 1) and DPPC: DPPE: CL (2: 1: 1) at the final concentration of 4 mM were evaluated in our experiments. The protein:lipid ratio of 1: 168 and 5 hours incubation period was set for protein incorporation. DSC measurements were carried out and thermograms were recorded (Figures 37 and 38, Tables 8 and 9).

As a positive control, the interaction between protein and liposome was monitored using DPPC liposomes. As previously observed, the presence of TcNTR induced changes in the transition enthalpy for DPPC liposomes (Table 8), as an undoubtedly proof of interaction. Although reproducible, the smaller shifts observed in this experiment can be explained as a consequence of a higher protein:lipid ratio, which could induce protein precipitation. Regarding

DPPC: DPPE (3: 1) lipid composition, no significant changes in the thermodynamic parameters were observed, however the shape of the curve changed, indicating a different lipid organization in the liposome (Figure 37).

For model membranes containing cardiolipin, a specific lipid of the mitochondrial membrane, we observed significant changes not only in the enthalpy but also in the temperature of transition, indicating strong interaction with the protein (Table 9). In the composition DPPC:DPPE:CL (2:1:1) the protein also changes the lipid organization in the liposome due to changes in the shape of the peak (Figure 38).

A significant change in the size distribution of the proteoliposomes from all the lipid compositions is observed at this molar ratio (Table 8 and 9). This is also an indicative of protein incorporation in the liposomes forming vesicles with different diameters.

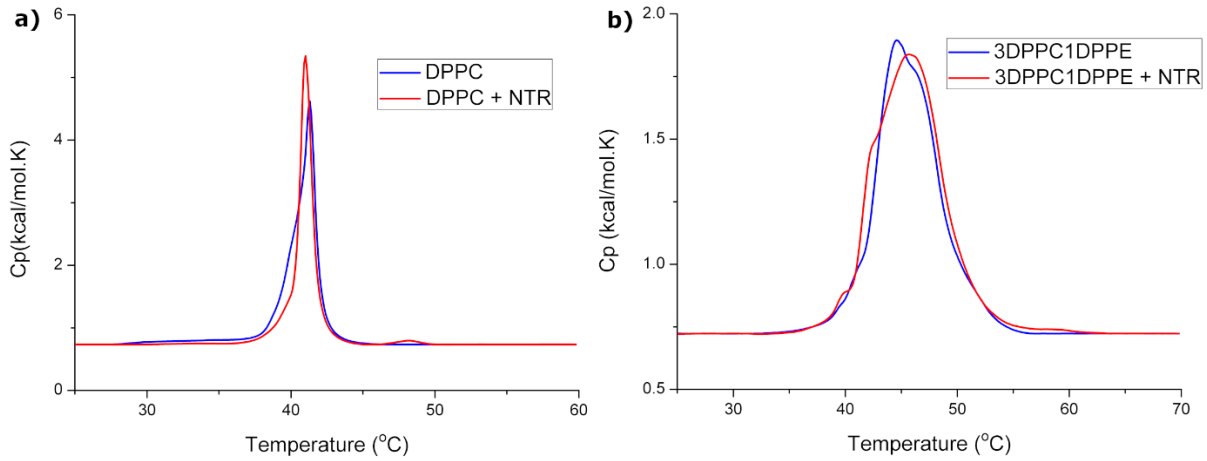

Figure 37: Thermograms obtained from liposomes of DPPC and DPPC: DPPE (3: 1) and the effect of incubation with the TcNTR protein, as verified by DSC.

Table 8: Thermodynamic parameters obtained by DSC and size evaluation of liposome samples by DLS for DPPC and DPPC: DPPE (3: 1) liposomes and the effect of incubation with TcNTR.

	DPPC Liposomes	**DPPC + NTR (1:168/5hrs)**	**DPPC:DPPE (3:1) Liposomes**	**DPPC:DPPE (3:1) + NTR (1:168/5hrs)**
Diameter (nm)	147 ± 1	290 ± 17	129 ± 1	1865 ± 601
Polidisp. Index	0.08	0.68	0.08	0.35
ΔH (kcal/mol)	7.58	6.53	8.02	8.07
Tc (ºC)	41.4	41.0	44.6	45.7
t½	1.51	0.92	5.56	6.35

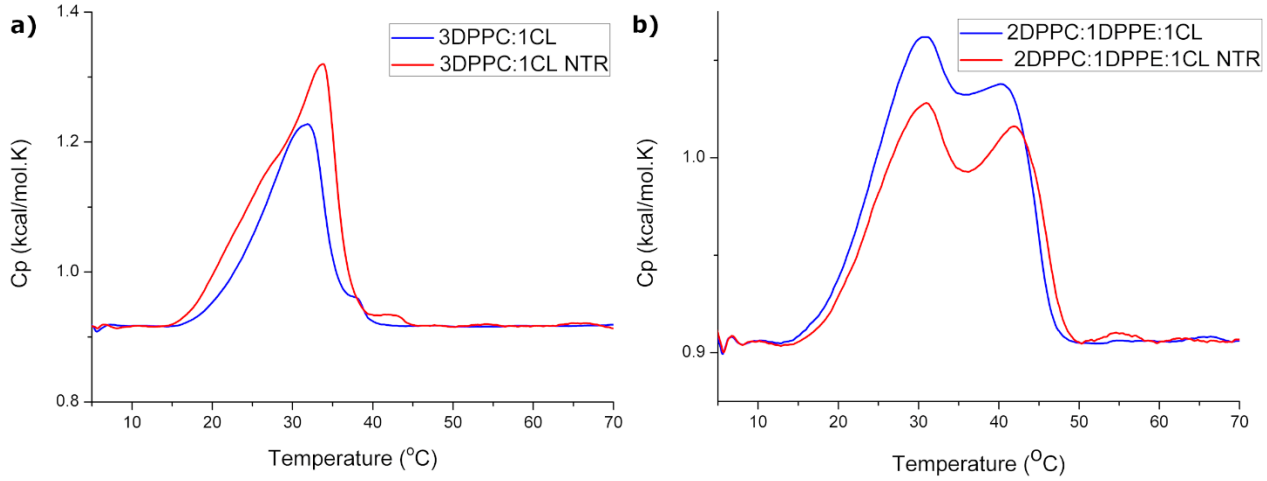

Figure 38: Thermograms obtained from liposomes of DPPC: CL (3: 1) and DPPC: DPPE: CL (2: 1: 1) and the effect of incubation with the TcNTR protein, as verified by DSC.

Table 9: Thermodynamic parameters obtained by DSC and size evaluation of liposome samples by DLS for liposomes of DPPC:CL (3:1) and DPPC: DPPE:CL (2:1:1) and the effect of incubation with TcNTR. * peak 1; ** peak 2.

	DPPC:CL 3:1 Liposomes	**DPPC:CL (3:1) + NTR (1:168/5hrs)**	**DPPC:DPPE:CL (2:1:1) Liposomes**	**DPPC:DPPE:CL (2:1:1) + NTR (1:168/5hrs)**
Diameter (nm)	132 ± 1	508 ± 106	145 ± 1	896 ± 323
Polidisp. Index	0.005	0.99	0.05	0.98
ΔH (kcal/mol)	3.04	4.52	2.53*	1.67*
			1.15**	0.77**
Tc (ºC)	31.9	33.9	30.1*	30.4*
			40.2**	42.2**
t½	7.8	9.9	10.5*	11.3*
			6.6**	6.2**

The interaction between TcNTR and lipids was also investigated by monitoring the influence of TcNTR72 on the surface tension of a lipid monolayer by using the pendant drop tensiometry method. Both DPPC and DPPC:DPPE:CL (2:1:1) membrane models were used (Figure 39). This method is based on the axissimetric analysis of the drop shape (ANDRADE et al., 2016). It was possible to calculate the exclusion pressure for the detergent free TcNTR72 in the values of 24.6 mN/m for DPPC and 28.9 mN/m for DPPC:DPPE:CL. The exclusion pressure is an initial surface pressure (directly proportional to the phospholipid concentration) above which no more protein could be inserted in the lipid layer. This parameter indicates the penetration power of the protein inside the lipid monolayer (ANDRADE et al., 2016;

WEINBERG et al., 2002). A higher surface pressure of TcNTR72 with the lipids DPPC:DPPE:CL confirms a higher interaction with a model membrane resembling the one from mitochondria.

Cardiolipin (CL) is a phospholipid esterified with 4 acyl chains instead of 2 from other phospholipids. It is close related to energy-transducing membranes being found in high concentrations at the inner mitochondrial membrane. Although not essential, cardiolipin is proved to interact with diverse inner mitochondrial membrane proteins. Crystal structures of protein complexes from the electron transport chain present tightly bound CL molecules suggesting an influence of this lipid in their proper folding. The presence of CL is also required for optimal activity of these protein complexes (PARADIES et al., 2014; SCHLAME; REN, 2009). A higher interaction observed in TcNTR with model membranes presenting cardiolipin corroborates the hypothesis of NTR functioning as a ubiquinone reductase (WILKINSON et al., 2008).

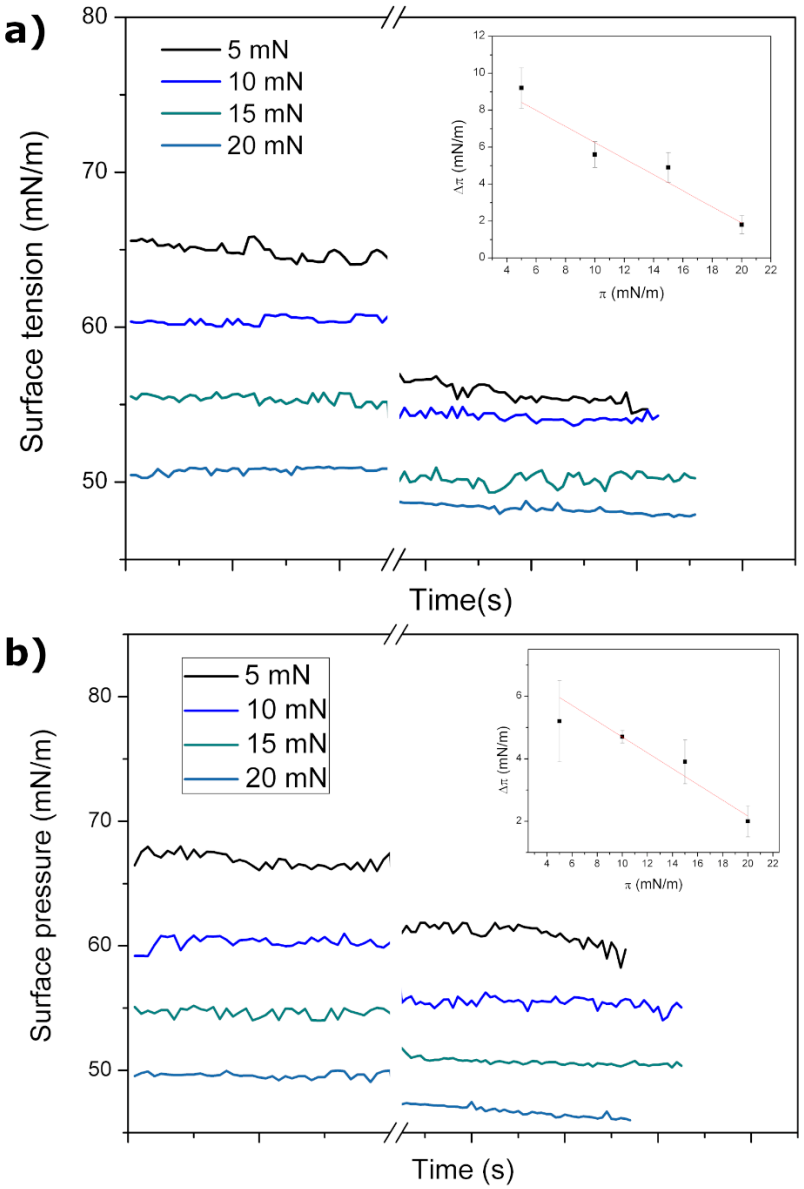

Figure 39: Profile of the drop in the surface tension of the lipid monolayer constituted of DPPC (a) and DPPC:DPPE:CL (2:1:1) molar ratio (b) after the insertion of the TcNTR, verified by the axissimetric analysis of the drop form.

In order to evaluate the role of detergents/lipids in protecting the FMN prosthetic group, we monitor the fluorescence of the FMN bound to TcNTR72 in presence of increasing concentrations of DPPC liposomes (Figure 40). It was observed that liposomes decreases the intensity of the FMN fluorescence and this phenomenon is dependent on lipid concentration. Those findings suggest that lipid binding occurs in the proximity of the FMN binding site.

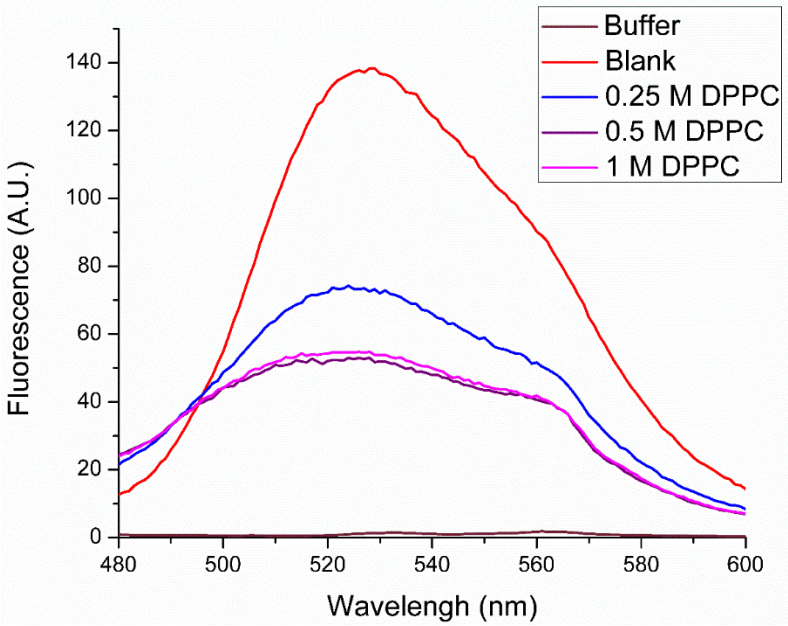

Figure 40: Emission spectra of the fluorescence for TcNTR72 and the influence of DPPC liposomes.

4.3. DSC analysis of TcNTR72

We initially performed the differential scanning calorimetry (DSC) assay of the TcNTR72 construct containing around 1% Triton X-100 detergent in the buffer solution (50 mM Tris pH 8.5 and 300 mM NaCl). An exothermic peak was observed at 60°C, which corresponds to the phase transition temperature of the detergent Triton X-100 (Figure 41). After removal of the detergent by treatment with the Calbiosorb resin, the exothermic peak is no longer observed, indicating that the procedure succeed in removing the majority of the detergent content. Another peak emerging around 120ºC was observed in both samples with and without detergent, being hypothesized that it would correspond to aggregates formed during sample heating.

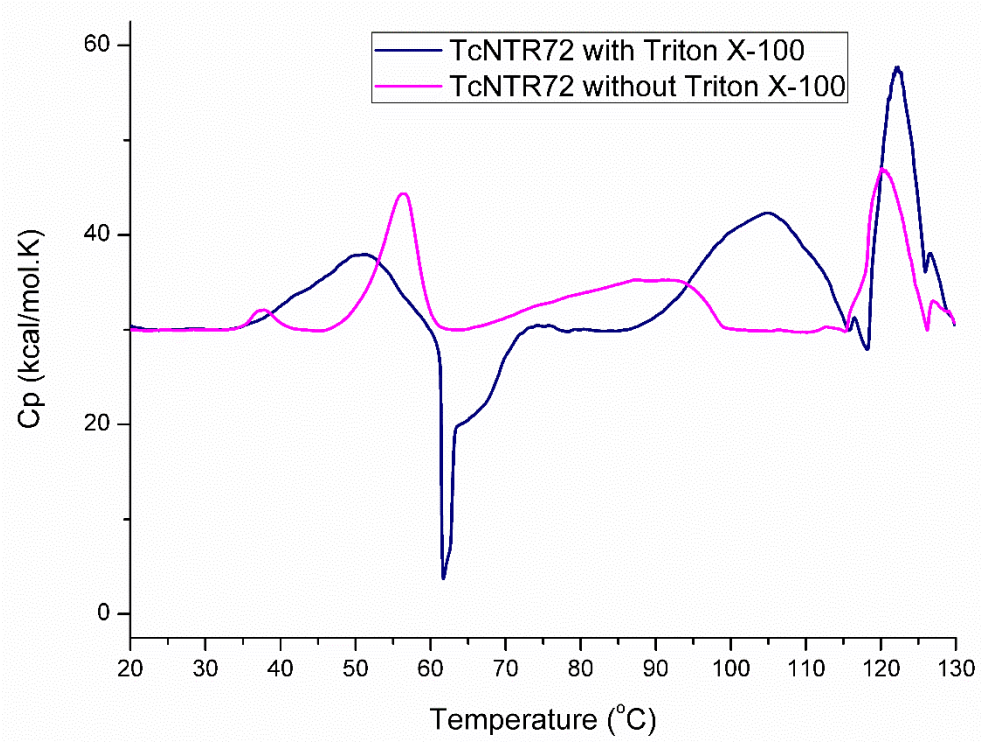

Figure 41: Differential scanning calorimetry of the construct TcNTR72 with and without the detergent Triton X-100. The large exothermic peak at 60ºC corresponds to the detergent phase transition.

DSC analyses of the detergent free TcNTR72 were performed in different concentrations. With a concentration of 0.95 mg/mL, there are two characteristic phase transition peaks, one around 55ºC and the second broader peak around 90ºC. Decreasing the protein concentration (from 0.95 to 0.25 mg/mL), the peak at 55ºC decreases in height and shifts to higher temperature while the second peak increases considerably (Figure 42). This concentration-dependent behavior can be explained as considering that TcNTR72 protein sample contains two populations/conformations, being one of them highly stable and predominant in lower concentrations. Other explanation relies on a different conformation adopted during sample heating, favored in lower concentrations. In all concentrations tested the sample aggregates during heating and its precipitation is observed as a peak at 120ºC. Further studies in order to better understand the thermal transitions observed for TcNTR are necessary.

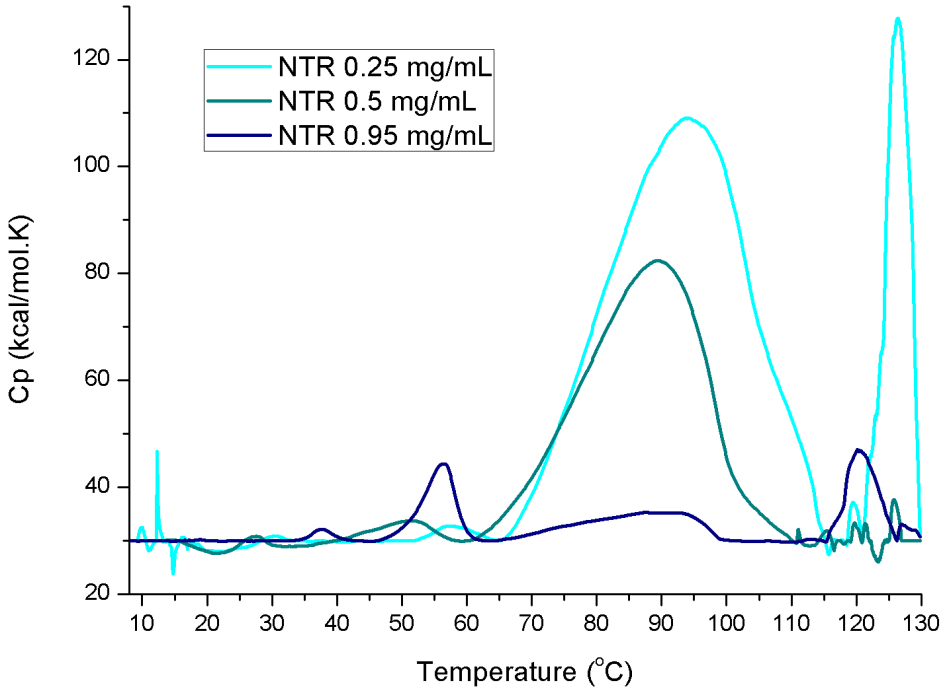

Figure 42: Thermograms (calorific capacity versus temperature) of TcNTR72 without detergent at 0.25, 0.5 and 0.95 mg/mL.

4.4. Crystalization experiments

The major goal of obtaining the full structure determination by single crystal X-ray diffraction was achieved. The conditions containing 0.1 M of potassium thiocyanate and 30% (w/w) PEG MME 2000 and 0.2 M of magnesium chloride, 0.1 M Tris pH 8.5 and 3.4 M 1,6-hexanediol using the protein solution incubated with 5 mM of 16-LPC had crystals confirmed to be proteic but diffracted at low resolution and could not be used for structure determination. Further approaches aiming to optimize the diffraction will be performed.

4.5. Structure models

Despite the use of different strategies, both *ab initio* and homology models were shown to display high level of structural similarity. A typical NTR structure comprises a four antiparallel β-strand (β_1- β_4) surrounded by variable number of α helices (α_1- α_{10}, Figure 43). Helices, represented by 5 and 6 in the *Thermus thermophilus* NADH oxidase structure, protrude from the core region of each molecule. There is an extensive dimer interface along the helix 7, and the C-terminal residues extend around the opposing monomer.

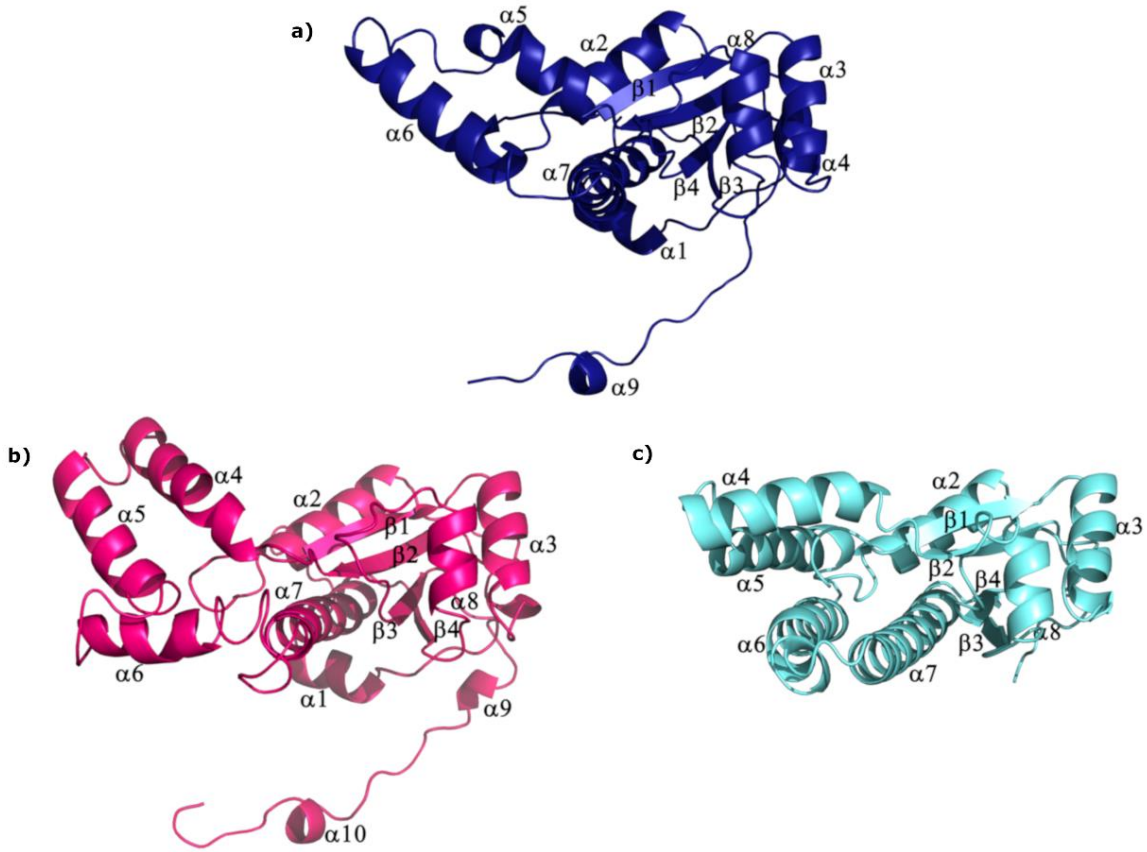

Figure 43: Cartoon representation of *Thermus termophilus* NADH oxidase (a) and TcNTR models (b, homology-based; c, ab initio).

The core formed by β-sheets surrounded by α-helices is found conserved in both I-TASSER and *ab initio* models which resembles the ones found in bacterial NTRs (Figure 42). In particular, the I-TASSER model built for TcNTR reveals the presence of a protuberant arm at the C-terminus region (residues 290 to 312, α9 and 10), important for dimerization. Moreover, the hydrophobic helix responsible for the majority of dimer interactions in bacterial NTRs (α7, comprising the residues 227 to 252, in TcNTR models) is also found in a similar position. Both findings corroborate to the hypothesis that TcNTRs is found in a dimeric conformation.

The superposition of Cα atoms between both models shows an RMSD of 4.6 Å (Figure 44). Worth mentioning that, even considering that the *ab initio* model covers a shorter fragment of the peptide chain, its N and C terminal residues were predicted to adopt similar folds in both models, supporting the hypothesis that removal of peptide stretches at the N- and C- terminus did not affect the quality of *ab initio* model. The region of the helices 4 and 5 could not be aligned (residues 167 to 193) but are reported to have high flexibility (ISAYEV et al.,

2012; MERKLEY; PARSON; DAGGETT, 2010). The final model would be composed of the N and C-terminal parts of the I-TASSER and the core from the ab initio models. However when building the dimer, using molecular dynamics, the FMN binding site was not conserved.

Figure 44: Cartoon representation in stereo view of TcNTR structure models. Superposition between the homology based (pink) and ab initio model (cyan) for TcNTR.

This way, a third model, also based on homology, was created using the server Swiss-Model in which it has a dimeric conformation. The putative FMN binding site composed by the conserved residues R88, S90, K92, Q145, E260 and R300 are positioned at the dimeric interface and interacting with the prosthetic group(Figure 45). This model is similar to the previous models, with a RMSD of 1.0 and 3.4 to the I-TASSER and QUARK models respectively.

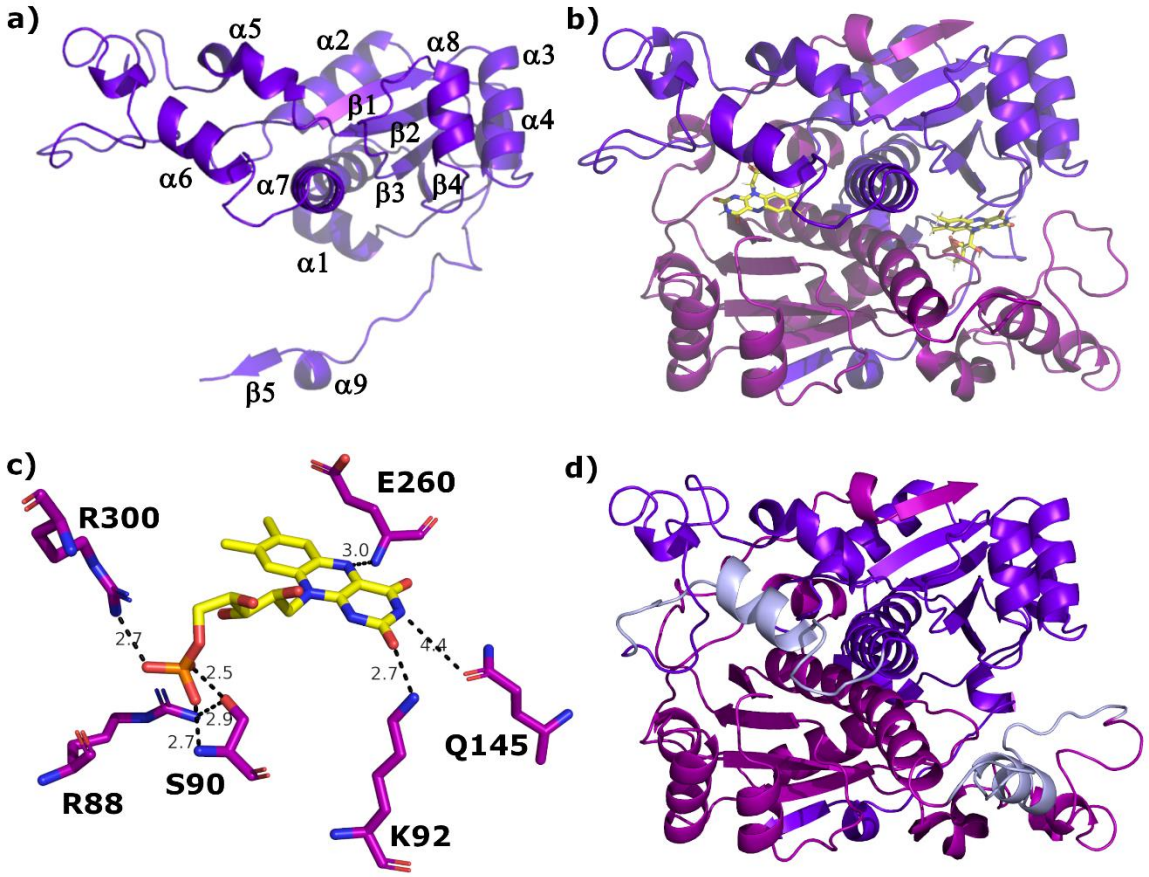

Figure 45: Cartoon representation of TcNTR model built in the server Swiss-Model as a monomer (a) and dimer contaning the prosthetic group FMN (b). (c) Conserved FMN binding site composed of the residues R88, S90, K92, Q145, E260 and R300. (d) Cartoon representation of TcNTR dimer highlighting the possible region responsible for membrane interaction.

The region comprising the residues 199 to 222, absent in most bacterial nitroreductases, but present and relatively conserved in NTRs from trypanosomatids (Figure 6 and 7) folds into helix α6. The region where this helix is inserted is considered flexible in other nitroreductases (ISAYEV et al., 2012; MERKLEY; PARSON; DAGGETT, 2010). It is also near the binding site for the prosthetic group FMN (figure 45). It is tempting to speculate whether this could be the region responsible for NTR:lipid interaction, since the loss of the FMN is observed in the purification without detergent. Besides being characteristic of trypanosomatid NTRs and found absent in bacterial NTRs, the hydrophobic surface could favor protein-membrane interactions. Further studies to better characterize TcNTR-membranes interactions are currently in progress.

Sequence alignment among trypanosomatid NTRs shows higher level of sequence identity than with bacterial NTRs (Figure 7), an evidence that trypanosomatid NTRS could share structural similarity. Deeper analyses are necessary to map the structural differences that

could explain the diversity of selectivity reported for the nitrocompounds among trypanosomatid NTRs.

5. Final remarks and future perspectives

Considering the lack of effective treatments for Chagas disease, which still affects millions of people worldwide, the study of the enzyme nitroreductase is essential for the understanding not only of the mechanism of action of the two drugs available, but also for the NTR role in the parasite metabolism and how NTR can be better exploited for drug design.

In this study two gene constructs, TcNTR72 (residues 72 to 312) and TcNTR78 (residues 78 to 312), were evaluated. The construct TcNTR72 showed itself more stable probably due to a proper folding of structural elements at the N-terminal stretch. The expression protocol was successfully optimized leading to higher yields of purified protein. Optimization of the purification protocol led to higher thermal stability on both constructs.

The presence of detergent during purification is required to keep structural integrity, thermal stability, and activity of TcNTR. This result led us to investigate a possible interaction with membranes. For the first time, TcNTR was shown to interact with model membranes, in particular the ones containing cardiolipin, a lipid specific of mitochondrion, the cellular location for tripanossomatids NTRs.

Molecular modelling suggests an α+β folding, characteristic of bacterial NTRs, despite the low sequential identity. The main difference is the fragment comprising residues 199 to 222 that is not present in the bacterial homologs. This region is hypothesized to be responsible for protein-membrane interaction.

Further studies, *in vitro* and *in silico,* for a better characterization of the TcNTR interaction with membranes will be performed. The complete structural characterization of TcNTR by single crystal X-ray diffraction was not achieved in this work and is important for a complete understanding of protein function and mechanism of selective activation of benznidazole and nifurtimox.

Bibliography

ANDRADE, M. A. R. et al. Pendant-drop method coupled to ultraviolet-visible spectroscopy: A useful tool to investigate interfacial phenomena. **Colloids and Surfaces A: Physicochemical**

and Engineering Aspects, v. 5, p. 305–311, 2016.

ARAÚJO, A. et al. Paleoparasitology of Chagas disease--a review. **Memorias do Instituto Oswaldo Cruz**, v. 104 Suppl, n. March, p. 9–16, 2009.

BERGER, M. JAMES; GAMBIN, J. STEVEN; HARRISON, C. STEPHEN; WANG, C. J. Structure and mechanism of DNA polymerases. **Nature**, v. 379, n. January, p. 225–232, 1996.

BERRY, J. D. et al. Measurement of surface and interfacial tension using pendant drop tensiometry. **Journal of Colloid and Interface Science**, v. 454, p. 226–237, 2015.

BOIVIN, S.; KOZAK, S.; MEIJERS, R. Optimization of protein purification and characterization using Thermofluor screens. **Protein Expression and Purification**, v. 91, n. 2, p. 192–206, 2013.

BOT, C. et al. Evaluating 5-nitrofurans as trypanocidal agents. **Antimicrobial Agents and Chemotherapy**, v. 57, n. 4, p. 1638–1647, 2013.

BRASIL; SAÚDE, M. DA. Doença de Chagas Aguda e distribuição espacial dos triatomíneos de importância epidemiológica, Brasil 2012 a 2016. **Boletim Epidemiológico**, v. 50, n. 2, p. 10, 2019.

CAMPOS, M. C. O. et al. Benznidazole-resistance in Trypanosoma cruzi: Evidence that distinct mechanisms can act in concert. **Molecular and Biochemical Parasitology**, v. 193, n. 1, p. 17–19, 2014.

CHENIOUR, M. et al. Evidence of proteolipid domain formation in an inner mitochondrial membrane mimicking model. **Biochimica et Biophysica Acta - General Subjects**, v. 1861, n. 5, p. 969–976, 2017.

CONNERS, E. E. et al. A global systematic review of Chagas disease prevalence among migrants. **Acta Tropica**, v. 156, p. 68–78, 2016.

COURA, R. Síntese histórica e evolução dos conhecimentos sobre a doença de chagas. **Clínica e terapêutica da doença de Chagas: uma abordagem prática para o clínico geral [online].**, 1997.

CROFTS, T. S. et al. Discovery and Characterization of a Nitroreductase Capable of Conferring Bacterial Resistance to Chloramphenicol. **Cell chemical biology**, p. 1–12, 2019.

DE OLIVEIRA, I. M.; HENRIQUES, J. A. P.; BONATTO, D. In silico identification of a new group of specific bacterial and fungal nitroreductases-like proteins. **Biochemical and Biophysical Research Communications**, v. 355, n. 4, p. 919–925, 2007.

DEMETZOS, C. Differential Scanning Calorimetry (DSC): A tool to study the thermal behavior of lipid bilayers and liposomal stability. **Journal of Liposome Research**, v. 18, n. 3, p. 159–173, 2008.

DRAZENOVIC, J. et al. Effect of lamellarity and size on calorimetric phase transitions in single component phosphatidylcholine vesicles. **Biochimica et Biophysica Acta - Biomembranes**, v. 1848, n. 2, p. 532–543, 2015.

DROZDETSKIY, A. et al. JPred4: A protein secondary structure prediction server. **Nucleic Acids Research**, v. 43, n. W1, p. W389–W394, 2015.

DUROWOJU, I. B. et al. Differential Scanning Calorimetry — A Method for Assessing the Thermal Stability and Conformation of Protein Antigen. **Journal of Visualized Experiments**, n. 121, p. 1–8, 2017.

ERICSSON, U. B. et al. Thermofluor-based high-throughput stability optimization of proteins for structural studies. **Analytical Biochemistry**, v. 357, n. 2, p. 289–298, 2006.

GARCIA-GUERRERO, M. C. et al. Crystal structure and mechanism of human carboxypeptidase O: Insights into its specific activity for acidic residues. **Proceedings of the National Academy of Sciences**, v. 115, n. 17, p. E3932–E3939, 2018.

GARCÍA-HUERTAS, P. et al. Prostaglandin F2α synthase in trypanosoma cruzi plays critical roles in oxidative stress and susceptibility to benznidazole. **Royal Society Open Science**, v. 4, n. 9, p. 170773, 2017.

GONÇALVES, C. S. et al. Revisiting the Trypanosoma cruzi metacyclogenesis: Morphological and ultrastructural analyses during cell differentiation. **Parasites and Vectors**, v. 11, n. 1, p. 1–14, 2018.

GUHL, F.; AUDERHEIDE, A.; RAMÍREZ, J. D. From ancient to contemporary molecular eco-epidemiology of Chagas disease in the Americas. **International Journal for Parasitology**, v. 44, n. 9, p. 605–612, 2014.

HALL, B. S. et al. Exploiting the drug-activating properties of a novel trypanosomal nitroreductase. **Antimicrobial Agents and Chemotherapy**, v. 54, n. 3, p. 1193–1199, 2010.

HALL, B. S.; BOT, C.; WILKINSON, S. R. Nifurtimox activation by trypanosomal type I nitroreductases generates cytotoxic nitrile metabolites. **Journal of Biological Chemistry**, v. 286, n. 15, p. 13088–13095, 2011a.

HALL, B. S.; BOT, C.; WILKINSON, S. R. Nifurtimox activation by trypanosomal type I nitroreductases generates cytotoxic nitrile metabolites. **Journal of Biological Chemistry**, v. 286, n. 15, p. 13088–13095, 2011b.

HALL, B. S.; MEREDITH, E. L.; WILKINSON, S. R. Targeting the Substrate Preference of a Type I Nitroreductase To Develop Antitrypanosomal Quinone-Based Prodrugs. **Antimicrobial Agents and Chemotherapy**, v. 56, n. 11, p. 5821–5830, 2012.

HALL, B. S.; WILKINSON, S. R. Activation of benznidazole by trypanosomal type I nitroreductases results in glyoxal formation. **Antimicrobial Agents and Chemotherapy**, v. 56, n. 1, p. 115–123, 2012.

HAWE, A. et al. Taylor dispersion analysis compared to dynamic light scattering for the size analysis of therapeutic peptides and proteins and their aggregates. **Pharmaceutical Research**, v. 28, n. 9, p. 2302–2310, 2011.

HECHT, H. J. et al. Crystal structure of NADH oxidase from Thermus thermophilus. **Nature**, v. 2, n. 12, p. 1109, 1995.

HUNTER, F. W. et al. Identification of P450 oxidoreductase as a major determinant of sensitivity to hypoxia-activated prodrugs. **Cancer Research**, v. 75, n. 19, p. 4211–4223, 2015.

ISAYEV, O. et al. In silico structure-function analysis of E. cloacae nitroreductase. **Proteins: Structure, Function and Bioinformatics**, v. 80, n. 12, p. 2728–2741, 2012.

JOHNSON, C. M. Differential scanning calorimetry as a tool for protein folding and stability. **Archives of Biochemistry and Biophysics**, v. 531, n. 1–2, p. 100–109, 2013.

KASZUBA, M. et al. Measuring sub nanometre sizes using dynamic light scattering. **Journal of Nanoparticle Research**, v. 10, n. 5, p. 823–829, 2008.

KROPF, S. P. Doença de Chagas, doença do Brasil: ciência, saúde e nação (1909-1962). p. 600, 2006.

LEE, B. Y. et al. Global economic burden of Chagas disease: a computational simulation model. v. 13, n. 4, p. 342–348, 2013.

MARBLESTONE, J. G. Comparison of SUMO fusion technology with traditional gene fusion systems: Enhanced expression and solubility with SUMO. **Protein Science**, v. 15, n. 1, p. 182–189, 2006.

MARIN-NETO, J. A. et al. The BENEFIT trial: testing the hypothesis that trypanocidal therapy is beneficial. **Mem Inst Oswaldo Cruz, Rio de Janeiro**, v. 104, n. May, p. 319–324, 2009.

MARTIN, D. L. et al. Trypanosoma cruzi survival following cold storage: Possible implications for tissue banking. **PLoS ONE**, v. 9, n. 4, 2014.

MARTÍNEZ-JÚLVEZ, M. et al. Structure of RdxA: an oxygen insensitive nitroreductase essential for metronidazole activation in Helicobacter pylori. **FEBS Journal**, v. 279, n. 23, p. 4306–4317, 2012.

MCCUSKER, E. C. et al. Structure of a bacterial voltage-gated sodium channel pore reveals mechanisms of opening and closing. **Nature Communications**, v. 3, p. 1–8, 2012.

MEJÍA-JARAMILLO, A. M. et al. Gene expression study using real-time PCR identifies an NTR gene as a major marker of resistance to benznidazole in Trypanosoma cruzi. **Parasites and Vectors**, v. 4, n. 1, p. 169, 2011.

MEJIA, A. M. et al. Benznidazole-resistance in trypanosoma cruzi is a readily acquired trait that can arise independently in a single population. **Journal of Infectious Diseases**, v. 206, n. 2, p. 220–228, 2012.

MERKLEY, E. D.; PARSON, W. W.; DAGGETT, V. Temperature dependence of the flexibility of thermophilic and mesophilic flavoenzymes of the nitroreductase fold. **Protein Engineering, Design and Selection**, v. 23, n. 5, p. 327–336, 2010.

MÜLLER, J.; HEMPHILL, A.; MÜLLER, N. Physiological aspects of nitro drug resistance in Giardia lamblia. **International Journal for Parasitology: Drugs and Drug Resistance**, v. 8, n. 2, p. 271–277, 2018.

MURAKAMI, M. T. et al. Structural studies of the Trypanosoma cruzi Old Yellow Enzyme:

Insights into enzyme dynamics and specificity. **Biophysical Chemistry**, v. 184, p. 44–53, 2013.

NILLIUS, D.; MÜLLER, J.; MÜLLER, N. Nitroreductase (GlNR1) increases susceptibility of Giardia lamblia and Escherichia coli to nitro drugs. **Journal of Antimicrobial Chemotherapy**, v. 66, n. 5, p. 1029–1035, 2011.

PÁDUA, R. A. P. et al. ThermoFMN - A thermofluor assay developed for ligand-screening as an alternative strategy for drug discovery. **Journal of the Brazilian Chemical Society**, v. 25, n. 10, p. 1864–1871, 2014.

PANTOLIANO, M. W. et al. Pantoliano Thermofluor.pdf. **Journal of Biomolecular Screening**, v. 6, n. 6, p. 429–440, 2001.

PARADIES, G. et al. Functional role of cardiolipin in mitochondrial bioenergetics. **Biochimica et Biophysica Acta - Bioenergetics**, v. 1837, n. 4, p. 408–417, 2014.

PARKINSON, G. N.; SKELLY, J. V; NEIDLE, S. Crystal Structure of FMN-Dependent Nitroreductase from Escherichia coli B : A. **J. Med. Chem.**, n. 43, p. 3624–3631, 2000.

PATTERSON, S.; WYLLIE, S. Nitro drugs for the treatment of trypanosomatid diseases: Past, present, and future prospects. **Trends in Parasitology**, v. 30, n. 6, p. 289–298, 2014.

PÉREZ-MOLINA, J. A. et al. Old and new challenges in Chagas disease. **The Lancet Infectious Diseases**, v. 15, n. 11, p. 1347–1356, 2015.

PÉREZ-MOLINA, J. A.; MOLINA, I. Chagas disease. **The Lancet**, v. 391, p. 82–94, 2017.

PEREZ, C. J.; LYMBERY, A. J.; THOMPSON, R. C. A. Reactivation of Chagas Disease: Implications for Global Health. **Trends in Parasitology**, v. 31, n. 11, p. 595–603, 2015.

PROSSER, G. A. et al. Creation and screening of a multi-family bacterial oxidoreductase library to discover novel nitroreductases that efficiently activate the bioreductive prodrugs CB1954 and PR-104A. **Biochemical Pharmacology**, v. 85, n. 8, p. 1091–1103, 2013.

ROBERTSON, L. J. et al. Trypanosoma cruzi: Time for International Recognition as a Foodborne Parasite. **PLoS Neglected Tropical Diseases**, v. 10, n. 6, p. 3–8, 2016.

ROLDÁN, M. D. et al. Reduction of polynitroaromatic compounds: The bacterial nitroreductases. **FEMS Microbiology Reviews**, v. 32, n. 3, p. 474–500, 2008.

SAAD, S. M. I.; POLICOVA, Z.; NEUMANN, A. W. Design and accuracy of pendant drop methods for surface tension measurement. **Colloids and Surfaces A: Physicochemical and Engineering Aspects**, v. 384, n. 1–3, p. 442–452, 2011.

SANTOS, S. P. et al. Thermofluor-based optimization strategy for the stabilization and crystallization of Campylobacter jejuni desulforubrerythrin. **Protein Expression and Purification**, v. 81, n. 2, p. 193–200, 2012.

SCHLAME, M.; REN, M. The role of cardiolipin in the structural organization of mitochondrial membranes. **Biochimica et Biophysica Acta - Biomembranes**, v. 1788, n. 10, p. 2080–2083, 2009.

SONG, H. N. et al. Crystal structure of the fungal nitroreductase Frm2 from Saccharomyces cerevisiae. **Protein Science**, v. 24, n. 7, p. 1158–1163, 2015.

SPINK, C. H. Differential Scanning Calorimetry. **Methods in Cell Biology**, v. 84, n. 7, p. 115–141, 2008.

STANAWAY, J. D.; ROTH, G. The Burden of Chagas Disease Estimates and Challenges. **Global Heart**, v. 10, n. 3, p. 139–144, 2015.

STEVERDING, D. The history of Chagas disease. **Parasites and Vectors**, v. 7, n. 1, p. 1–8, 2014.

STUDIER, F. W. Protein production by auto-induction in high density shaking cultures. **Protein expression and purification**, v. 41, n. 1, p. 207–234, 2005.

TEIXEIRA, D. E. et al. Interactive Multimedia to Teach the Life Cycle of Trypanosoma cruzi, the Causative Agent of Chagas Disease. **PLoS Neglected Tropical Diseases**, v. 6, n. 8, p. e1749, 2012.

VOAK, A. A. et al. An essential type I nitroreductase from leishmania major can be used to activate leishmanicidal prodrugs. **Journal of Biological Chemistry**, v. 288, n. 40, p. 28466–28476, 2013.

WANG, B. et al. Crystal structures of two nitroreductases from hypervirulent Clostridium difficile and functionally related interactions with the antibiotic metronidazole. **Nitric Oxide - Biology and Chemistry**, v. 60, p. 32–39, 2016.

WATERHOUSE, A. et al. SWISS-MODEL: Homology modelling of protein structures and complexes. **Nucleic Acids Research**, v. 46, n. W1, p. W296–W303, 2018.

WEIDS, A. J. et al. Distinct stress conditions result in aggregation of proteins with similar properties. **Scientific Reports**, v. 6, 2016.

WEINBERG, R. B. et al. Interfacial exclusion pressure determines the ability of apolipoprotein A-IV truncation mutants to activate cholesterol ester transfer protein. **Journal of Biological Chemistry**, v. 277, n. 24, p. 21549–21553, 2002.

WILKINSON, S. R. et al. A mechanism for cross-resistance to nifurtimox and benznidazole in trypanosomes. **Proceedings of the National Academy of Sciences**, v. 105, n. 13, p. 5022–5027, 2008a.

WILKINSON, S. R. et al. A mechanism for cross-resistance to nifurtimox and benznidazole in trypanosomes. **Proceedings of the National Academy of Sciences**, v. 105, n. 13, p. 5022–5027, 2008b.

XU, D.; ZHANG, Y. Ab initio protein structure assembly using continuous structure fragments and optimized knowledge-based force field. **Proteins: Structure, Function and Bioinformatics**, v. 80, n. 7, p. 1715–1735, 2012.

XU, D.; ZHANG, Y. Toward optimal fragment generations for ab initio protein structure assembly. **Proteins: Structure, Function and Bioinformatics**, v. 81, n. 2, p. 229–239, 2013.

YANG, J. et al. The I-TASSER suite: Protein structure and function prediction. **Nature Methods**, v. 12, n. 1, p. 7–8, 2014.

ZHOU, L. et al. ALDH2 mediates 5-nitrofuran activity in multiple species. **Chemistry and Biology**, v. 19, n. 7, p. 883–892, 2012.